Research Square

Preprints are preliminary reports that have not undergone peer review.
They should not be considered conclusive, used to inform clinical practice,
or referenced by the media as validated information.

An elite allele TaNPF7.6-A1mod enhances nitrogen use efficiency and grain yield in wheat

Weigang Xu

xuwg1958@163.com

College of Agronomy, Henan Agricultural University

Di Jiang

Henan Agricultural University

Chaojun Peng

Institute of Crops Molecular Breeding, Henan Academy of Agricultural Sciences

https://orcid.org/0000-0002-5574-3552

Yan Li

Institute of Crops Molecular Breeding, Henan Academy of Agricultural Sciences

Chen Gong

Institute of Crops Molecular Breeding, Henan Academy of Agricultural Sciences

Yuhui Fang

Henan Academy of Agricultural Sciences

Xingyu Zhang

Henan Agricultural University

Zhaoyang Wang

Henan Agricultural University

Xinnan Wang

Henan Agricultural University

Lin Hu

Wheat Research Institute, Henan Academy of Agricultural Sciences, Henan

Xueli Qi

Wheat Research Institute, Henan Academy of Agricultural Sciences, Henan

Article

Keywords:

Posted Date: March 8th, 2026

DOI: https://doi.org/10.21203/rs.3.rs-9009137/v1

License: This work is licensed under a Creative Commons Attribution 4.0 International License.
Read Full License

Additional Declarations: There is **NO** Competing Interest.

Version of Record: A version of this preprint was published at Nature Communications on September 9th, 2026. See the published version at https://doi.org/10.1038/s41467-026-76836-2.

An elite allele *TaNPF7.6-A1^{mod}* enhances nitrogen use efficiency and grain yield in wheat

Di Jiang[1,2,3,4], Chaojun Peng[2,3,4], Yan Li[2,3], Chen Gong[2,3], Yuhui Fang[2,3], Xingyu Zhang[1], Zhaoyang Wang[1,2,3], Xinnan Wang[1,2,3], Lin Hu[2,3], Xueli Qi[2,3,*] and Weigang Xu[1,2,3,*]

[1]State Key Laboratory of Wheat and Maize Crop Science, Collaborative Innovation Center of Henan Grain Crops, College of Agronomy, Henan Agricultural University, Zhengzhou, Henan, China

[2]National Engineering Laboratory of Wheat, Key Laboratory of Wheat Biology and Genetic Breeding in Central Huanghuai Area, Ministry of Agriculture, Henan Key Laboratory of Wheat Germplasm Resources Innovation and Improvement, Institute of Crops Molecular Breeding, Henan Academy of Agricultural Sciences, Zhengzhou, Henan, China

[3]The Shennong laboratory, Zhengzhou, Henan, China

[4]These authors contributed equally to this work

*Corresponding authors: Weigang Xu (xuwg1958@163.com), Xueli Qi (xueliqi888@163.com)

ABSTRACT

Breeding wheat varieties with high nitrogen use efficiency (NUE) effectively reduces threats to the ecological environment and production costs. Here, this study identifies *TaNPF7.6-A1* as a positive regulator of NUE in wheat through candidate-gene and genome-wide association studies. A widely conserved polymorphism in the coding region of *TaNPF7.6-A1* produces an allele, *TaNPF7.6-A1^{mod}*, that has a higher transcriptional level and nitrate transport activity, resulting in greater NUE than *TaNPF7.6-A1^{lan}*. We also discovered a novel mechanism of *TaEIL3-TaJAZ1-TaNPF7.6-A1* regulating NUE in wheat: TaNPF7.6-A1^{mod} interacts more strongly with TaJAZ1 and promotes the retention of nuclear-localized TaJAZ1 in the cytoplasm

than TaNPF7.6-A1^{lan} does. TaJAZ1 interact with TaEIL3 and repress TaEIL3 binding to the *TaNPF7.6-A1^{mod}* promoter, thereby influencing alleles' expression and causing phenotypic differences. *TaNPF7.6-A1*^{mod} also shows significant geographical distribution aggregation globally and has undergone continuous positive selection during the breeding process. Overall, this study provides molecular and evolutionary insights into the regulation of NUE.

Nitrogen fertilizers are one of the most important developments in modern agricultural practices, playing a crucial role in ensuring global food security. However, their widespread application has led to environmental issues such as soil acidification, water eutrophication, and ozone layer depletion, posing significant challenges to sustainable agriculture[1,2]. Despite the adverse environmental impacts associated with nitrogen fertilizers, reducing their application rates is not a viable option. This is primarily due to the escalating global demand for food and the heavy reliance of current crop varieties on nitrogen inputs[3]. One practical approach to addressing this dilemma is to breed crop varieties with enhanced nitrogen use efficiency (NUE) through genetic improvement.

As described by Moll et al. (1982)[4], NUE comprises two component traits: nitrogen uptake efficiency (NUpE) and nitrogen utilization efficiency (NUtE). NUpE reflects the ability of plants to absorb available nitrogen, and is closely related to root structure, nitrogen transport capacity, and the external environment. Recently, several genes that regulate wheat root structure have been identified. TaWFZP directly activates genes related to root development and nitrate uptake by interacting with TaSYD, and it regulates the expression of genes reacted to roots and nitrogen, thereby promoting nitrogen utilization[5]. TaNLP3 activates *TaNRT2.1*, thereby promoting nitrate uptake[6]. In *Arabidopsis*, the binding strength of NRT2.1 with NAR2.1

is regulated by phosphorylation, thereby affecting NUpE[7]. NUtE reflects the grain yield produced per unit of absorbed nitrogen. *TaNAM* can affect wheat NUtE and positively regulate nitrogen redistribution, thereby influencing the grain protein content (GPC)[8]. Overexpression of *TaTIP4.1* increases the vacuolar $NH4^+$ efflux rate, improves the NUE of senescent leaves, and increases grain nitrogen accumulation (GNA)[9]. However, as yield increases, the grain nitrogen concentration often decreases due to the "dilution effect", resulting in a generally negative correlation between yield and grain nitrogen content[10]. When improving NUE, it is important to consider the coordinated improvement of GNA to achieve a high yield and quality. In summary, NUpE and NUtE together determine the overall level of NUE, which is reflected in nitrogen accumulation amount (NAA), a range of physiological, developmental and agronomic traits.

The NPF family of plant nitrate transporters is one of the largest and most functionally diverse. In recent years, they have become an important subject in the study of the molecular mechanisms influencing NUE[11,12]. Wheat contains 331 *NPF* genes, indicating a high degree of expansion and differentiation within this gene family[12]. However, although wheat contains many *NPF* genes, only *TaNPF6.2* has been reported to enhance nitrogen absorption efficiency, resulting in higher tiller numbers, longer panicles, a greater number of grains per panicle, and increased 1000-grain weight[13]. The *TaNPF2.12 TT* allele significantly increases nitrogen use efficiency under low-nitrogen conditions by raising nitrogen content in leaves and grains[14]. Nevertheless, progress in delineating the regulatory network through which *TaNPFs* control wheat NUE remains limited, and the precise mechanisms of their action are unclear.

In this study, we performed CGAS and GWAS for two NUE-related traits, nitrogen accumulation amount (NAA) and grain nitrogen accumulation (GAN), in 244 wheat accessions.

We identified *TaNPF7.6-A1* as a novel gene that coordinates the regulation of wheat NUE and yield, and we discovered the superior *TaNPF7.6-A1*^{mod} allele, which achieves dual functional optimization by combining elevated transcript abundance and enhanced transporter activity. Furthermore, we found that expressional differences of *TaNPF7.6-A1* alleles are not due to transcriptional regulation, but are instead determined by the strength of protein interactions, a previously unrecognized mechanism. *TaNPF7.6-A1*^{mod} exhibits significant geographical distribution aggregation globally and has undergone continuous positive selection during the breeding process. This study not only clarifies the key function of the *TaNPF7.6-A1*^{mod} in regulating wheat NUE and reveals a new mechanism whereby the intensity of protein interactions affects the expression level. It also provides gene resources for breeding high-yielding, high-quality, and environmentally friendly wheat.

RESULTS

Identification of candidate gene *TaNPF7.6-A1* for NAA and GAN

To identify loci for NAA and GAN, we measured their phenotypes in 244 wheat accessions. We performed a CGAS using 1,053 effective SNPs located within a 4,000 bp genomic region spanning 2,000 bp upstream and 2,000 bp downstream of each of the 331 *NPF* family members (Supplementary Data 1). Of the fifteen significant SNPs identified by the CGAS, six were repeatedly associated with multiple environments and traits. One of these, *AX-111715806*, was located within *TraesCS1A02G197600* on chromosome 1A and accounted for total phenotypic variance of these traits ranging from 13.06% to 32.94% for these traits (Fig. 1a, Supplementary Data 2). We also performed GWAS for NAA and GAN, as well as for their best linear unbiased prediction (BLUP) values in the same 244 wheat accessions, identifying 281 SNPs that were

significantly associated with the two traits (Fig. 1b, c). Two significant SNP, *AX-111733802* and *AX-89423870*, were located 1.7 Mb and 0.6 Mb upstream of *TraesCS1A02G197600* (Supplementary Data 3). To further identify candidate genes, we assessed the transcriptional expression patterns of the 15 *NPF* candidate genes in response to varying nitrogen levels in the shoots and roots of wheat seedlings. Our analysis revealed that *TraesCS1A02G197600* (*TaNPF7.6-A1*) was the only gene induced in both the shoot and root under different nitrogen concentration conditions (Fig. 1d). These results suggest that *TaNPF7.6-A1* plays a crucial role in influencing wheat NUE.

We identified the superior alleles of eight *NPF* genes based on the genotypes of these genes and the trait phenotypes of 244 wheat accessions (Supplementary Data 4 and 5). We also analyzed the composition of superior alleles in 20 wheat varieties with different NUEs. Wheat varieties with high NUE had more superior alleles. For example, the high-NUE variety, Zhengmai 1860, had the greatest number of superior alleles (eight), whereas the relatively high-NUE varieties, Zhengmai 7698 and Jimai 30, had between five and six superior alleles (Fig. 1e and Supplementary Data 6). These results suggest that higher wheat NUE is associated with a greater number of superior *NPF* alleles.

Moreover, we expanded our analysis by comparing the *TaNPF7.6-A1* coding sequences across twenty wheat varieties. This comparison revealed a conserved and specific SNP at 1292 bp in the coding region, resulting in a change from valine to alanine at the amino acid position 431 (Fig. 1f). Based on the CAPS marker genotypes of 244 wheat accessions, we identified two alleles: *TaNPF7.6-A1*^{mod} and *TaNPF7.6-A1*^{lan}, the former allele exhibited higher NAA, GNA, and GY than the latter allele under both NN (normal nitrogen) and LN (low nitrogen) conditions (Fig. 1g, h and Supplementary Fig. 1a-c). We then examined the expression levels of *TaNPF7.6-*

A1 in twenty wheat varieties. The results showed that *TaNPF7.6-A1^{mod}* had higher NUE and higher expression levels than *TaNPF7.6-A1^{lan}* (Fig. 1i and Supplementary Data 6). In conclusion, the two alleles appear to be regulated differently at the transcriptional level and are positively correlated with NUE.

High *TaNPF7.6-A1^{mod}* levels confer advantages in NUE and grain yield under field conditions

To determine the impact of different *TaNPF7.6-A1* alleles on wheat NUE, we developed a pair of near-isogenic lines with *TaNPF7.6-A1^{mod}* and *TaNPF7.6-A1^{lan}* alleles through repeated backcrossing and the use of a CAPS marker. The receptor and donor parents were Zhengmai 9023 (high NUE) and Baibiansui (low NUE), respectively (Supplemental Fig. 1d-j). NIL^{mod} exhibited higher *TaNPF7.6-A1* expression levels and more favorable agronomic traits than NIL^{lan} (Fig. 2a and Supplemental Fig. 2a). These agronomic traits include a developed root system, increased biomass, improved aboveground nitrogen accumulation, enhanced yield per plant and increased grain nitrogen accumulation in wheat (Table 1 and Supplemental Fig. 2b-f). Therefore, *TaNPF7.6-A1^{mod}* is a superior allele for regulating NUE in wheat.

We characterized the tissue-wide expression pattern of *TaNPF7.6-A1^{mod}* in various wheat tissues at the different developmental stages. We found that *TaNPF7.6-A1^{mod}* is highly expressed in the basal part of the tiller after the jointing stage and in the flag leaves and spike after the flowering stage (Supplemental Fig. 3a, b). These results suggest that *TaNPF7.6-A1^{mod}* appears to dynamically modulate its “working intensity” (expression level) in response to environmental nitrogen availability and developmental stages. To verify the role of *TaNPF7.6-A1^{mod}* in NUE, we generated *TaNPF7.6-A1^{mod}* overexpression lines with the constitutive *ZmUbi1* promoter in the Zhengmai 7698 (ZM7698) background, as well as *TaNPF7.6-A1^{mod}*

knockout plants using CRISPR-Cas9 in ZM7698. These lines carry insertions or deletions that cause frameshifts in all three homoeologs (Supplemental Fig. 3c, d). We examined the phenotypes of those lines under the NN and LN conditions at three stages: jointing, flowering with high *TaNPF7.6-A1*^{mod} expression and maturity. As expected, there were significant differences in phenotypic growth between the transgenic lines and the wild-type plants. The Z-NO lines exhibited improved growth at various stages in the field, whereas the z-nc lines displayed evident growth defects. Compared to ZM7698, the Z-NO lines had more tillers and a better-developed root system at the jointing stage, particularly when subjected to LN treatment (Fig. 2b). The aboveground dry weight and the plant nitrogen accumulation increased in the Z-NO lines, while the exact opposite phenotypes were observed in the z-nc1 and z-nc2 plants (Table 1). At the flowering stage, the nitrogen accumulation in the spike and straw of the Z-NO lines increased significantly compared to ZM7698 (Data 1). Under NN treatment, the aboveground nitrogen accumulation in Z-NO1 and Z-NO2 increased by an average of 35.21% and 39.70%, respectively. Under the LN treatment, it increased by an average of 23.86% and 27.27%, respectively (Supplemental Fig. 3e, f). These results indicate that the increase in aboveground nitrogen accumulation at the flowering stage is primarily due to the combined effect of the spike and straw. At the maturity stage, Z-NO1 and Z-NO2 exhibited a significant increase in aboveground nitrogen accumulation (Supplemental Fig. 3g, h). Although the plant height increased (Supplemental Fig. 3i), there was no significant change in straw nitrogen accumulation (Table 1 and Supplemental Fig. 3j). Grain nitrogen accumulation increased significantly, especially under the NN field, averaging 25.64% and 25.22% higher than that in ZM7698, and increasing by an average of 19.36% and 25.17% under the LN field, respectively (Table 1, Supplemental Fig. 3k). In conclusion, the expression pattern of *TaNPF7.6-A1*^{mod} varies

in response to environmental changes, resulting in distinct physiological effects in different parts of the plant. Under low nitrogen conditions, *TaNPF7.6-A1^{mod}* expression increases nitrogen absorption but restricts overall plant growth. In fields with normal nitrogen supplies, *TaNPF7.6-A1^{mod}* facilitates the efficient utilization of nitrogen and promotes its transport to grains.

We further analyzed the yield components of different lines, and found that when Z-NO1 and Z-NO2 plants were planted at low densities in the field, the average yield per plant in the NN and LN field all increased (Fig. 2c). Furthermore, an analysis of three yield factors revealed that the Z-NO lines showed a significant increase in effective spike number. However, there was no difference in grain number per spike, 1000-grain weight (Fig. 2d-f), or panicle length (Supplemental Fig. 3l). To determine whether the function of *TaNPF7.6-A1^{mod}* is conserved in different genetic contexts, *TaNPF7.6-A1^{mod}* overexpression lines F-NO1 and F-NO2, and *TaNPF7.6-A1^{mod}* mutant lines (f-nc1 and f-nc2) were also constructed in the Fielder background (Supplemental Fig. 4a, b). Similar trends were observed between the transgenic Fielder lines and the mutant Fielder plants. The F-NO lines showed significantly better growth in the NN and LN fields than the wild-type, while the f-nc line showed the opposite trend (Supplemental Fig. 4c). The aboveground nitrogen accumulation of the F-NO lines was also significantly higher (Supplemental Fig. 4d, e). This increased nitrogen accumulation was also distributed to the grains (Supplemental Fig. 4f, g), and increased the yield per plant by increasing the number of effective spikes (Supplemental Fig. 4h). These results all indicate that *TaNPF7.6-A1^{mod}* is a positive regulator of NUE, *TaNPF7.6-A1^{mod}* overexpression increases yield by raising the number of effective spikes.

TaNPF7.6-A1^{mod} is a positive regulator of wheat NO_3^- uptake and translocation capacity

Crops primarily absorb and utilize two forms of nitrogen: NH_4^+ and nitrate NO_3^-. We then evaluated the expression patterns of *TaNPF7.6-A1* in the roots and shoots of wheat seedlings grown with different nitrogen sources. Compared to the NH_4^+ treatment, the NO_3^- treatment resulted in increased expression in the roots and shoots, with higher expression levels observed in environments with a high NO_3^- concentration (Fig. 3a, b). Furthermore, we examined the GUS signal in *pTaNPF7.6-A1*::GUS *Arabidopsis thaliana* transgenic seedlings cultivated on a modified 1/2 MS medium containing either 2 mM NH_4Cl or 2 mM KNO_3 as the sole nitrogen source for seven days. GUS signals were only detected on the leaves of seedlings grown on a medium containing KNO_3 as the sole nitrogen source (Supplemental Fig. 5a, b). These results suggest that *TaNPF7.6-A1* mainly responds to NO_3^-.

To determine the subcellular localization of TaNPF7.6-A1, the TaNPF7.6-A1-GFP fusion protein was expressed in wheat protoplasts and tobacco leaves. Both were found to be located on the tonoplast, as revealed by colocalization assays with the tonoplast marker AtINT1[15]. This suggests that TaNPF7.6-1A might have a transport function (Supplemental Fig. 5c, d). Next, we examined whether *TaNPF7.6-A1*^{lan} and *TaNPF7.6-A1*^{mod} encode a functional nitrate transporter by using the *Xenopus laevis* oocyte heterologous expression system (Supplemental Fig. 6). Under ^{15}N-nitrate concentrations of 0.25 and 10 mM, oocytes expressing *TaNPF7.6-A1*^{lan} and *TaNPF7.6-A1*^{mod} exhibited higher ^{15}N abundance than water-injected controls. At the same concentration of NO_3^-, both *TaNPF7.6-A1*^{lan}- and *TaNPF7.6-A1*^{mod}-injected oocytes were larger at pH 5.5 than at pH 7.4. Meanwhile, the abundance of ^{15}N in oocytes injected with *TaNPF7.6-A1*^{mod} was higher than in oocytes injected with *TaNPF7.6-A1*^{lan} at the same pH (Fig. 3c). Therefore, we believe that the response of *TaNPF7.6-A1*^{mod} responds more strongly to nitrate than *TaNPF7.6-A1*^{lan} does. Next, we examined how *TaNPF7.6-A1* varies among

different wheat alleles under the same conditions. Compared with NIL^{lan} plants, NIL^{mod} plants exhibited improved growth (Fig. 3d and Supplemental Fig. 7a-f), increased nitrogen enrichment (Fig. 3e, f), and enhanced nitrate absorption and transport (Fig. 3g, h). These results, demonstrated by both long-term hydroponic culture and short-term ^{15}N labelling, reveal that *TaNPF7.6-A1^{mod}* is an elite allele for enhancing NUE by increasing nitrogen absorption and transport.

To further investigate the effect of *TaNPF7.6-A1^{mod}* on the growth of wheat seedlings, we examined the growth phenotypes of ZM7698, Z-NO, and z-nc plants grown in a hydroponic culture medium with different N supply conditions over a period of 14 days: Normal nitrate (NN, 2 mM NO_3^-) and low nitrate (LN, 0.2 mM NO_3^-). The results showed that *TaNPF7.6-A1^{mod}* overexpression promoted wheat shoot and root growth under two conditions. It also increased fresh shoot and root weight, as well as deeper root length, wider root surface area, and root volume, compared to ZM7698. Meanwhile, the z-nc lines exhibited severe growth retardation (Figure 3i and Supplemental Fig. 8a-f). The nitrogen content of the shoots and roots of the Z-NO1 and Z-NO2 lines was significantly higher than that of the variety ZM7698. In contrast, the nitrogen content of the z-nc1 and z-nc2 lines was significantly lower (Fig. 3j, k). Consistently, the uptake and transport rate of ^{15}N-nitrate were determined using a ^{15}N-KNO_3 assay. Compared to ZM7698, the average influx rate of Z-NO1 and Z-NO2 plants under NN conditions increased by 11.91% and 13.87%, respectively. Under the LN conditions, the influx rate increased by an average of 10.45% and 11.40%, respectively (Fig. 3l). Under NN conditions, the average $^{15}NO_3^-$ transport from the roots to the shoots of the Z-NO1 and Z-NO2 plants increased by 10.92% and 15.55%, respectively. Under LN conditions, the average $^{15}NO_3^-$ transport from roots to shoots of the Z-NO lines increased by 10.72% and 12.83%, respectively

(Fig. 3m). Overexpression of *TaNPF7.6-A1*^{mod} increased $^{5}NO_3^-$ uptake by roots and $^{5}NO_3^-$ transport from roots to shoots; conversely, the *TaNPF7.6-A1*^{mod} mutant reduced nitrate uptake and transport in wheat. Notably, *TaNPF7.6-A1*^{mod} is more responsive to higher nitrate conditions. Similar trends were observed among F-NO1, F-NO2, f-nc1, f-nc2 and Fielder plants (Supplemental Fig. 9 and 10). These results suggest that *TaNPF7.6-A1* modulates the nitrate uptake, but not ammonium uptake. Overexpression of *TaNPF7.6-A1*^{mod} enhances the root system growth, stimulates nitrate uptake, and improves nitrate transport to the aboveground tissues.

TaEIL3 binds to and activates the promoter of *TaNPF7.6-A1*, regulating the expression of *TaNPF7.6-A1* in wheat

Previously, we demonstrated that *TaNPF7.6-A1* regulates NUE via transcription, with two alleles exhibiting different levels of transcription. We therefore extracted a 2000 bp of sequence upstream of the transcription start codon ATG as promoter region from twenty wheat varieties, and we observed that all *TaNPF7.6-A1*^{mod} members have the same promoter. Only 10 SNPs were found in the promoter region of *TaNPF7.6-A1*^{mod} compared to *TaNPF7.6-A1*^{lan} (Supplemental Fig. 11a). To reveal the regulation of the *TaNPF7.6-A1* promoter, we used Megadock software and AlphaFold to construct a three-dimensional (3D) model of the *TaNPF7.6-A1*^{mod} promoter sequence. We then compared the quality of the *TaNPF7.6-A1*^{mod} promoter 3D structure with that of the 3,396 digitized wheat transcription factors[16,17]. We considered the predictive 3D model to be successful when it achieved a score of 100% and could fully replace the actual results. Five transcription factors were successful in this regard, and their interaction scores were also higher than those of the positive controls (*p53* and pGADT7-p53m). Of these five genes, *TaEIL3* (*TraesCS7B02G145400.1*) not only has a high

interaction score and a 100% 3D modeling score. Its transcriptional level in the roots and shoots of wheat seedling under four nitrogen conditions shows the same nitrogen response pattern as *TaNPF7.6-A1* (Supplemental Data 7 and Supplemental Fig. 11b, c). The transcriptional activation and nuclear localization activities of TaEIL3 as a transcription factor were validated in yeast (Supplemental Fig. 11d-f).

To validate the potential association of TaEIL3 binding to *TaNPF7.6-A1*, we performed Y1H assays and found that TaEIL3 specifically binds to the P3 region, which contains a potential gagaTACATgt motif (Fig. 4a). This motif exhibits no base differences in the *TaNPF7.6-A1*^{mod} and *TaNPF7.6-A1*^{lan} promoters. Furthermore, we used PlantPAN 4.0 to predict four other transcription factors. It was found that the possible binding motifs (Similar Score = 1) also showed no base differences in the two alleles (Supplemental Fig. 12). Next, we designed a FAM-labeled probe according to the P3 sequence to perform an electrophoretic mobility shift assay. The EMSA results showed a shift in the electrophoretic mobility of the FAM-labeled probe. Adding different concentrations of competing probes caused the binding bands to weaker, and the mutated competing probe failed to produce the same effect (Fig. 4b). Meanwhile, we assessed the impact of the TaEIL3 protein on the promoter activity of the two *TaNPF7.6-A1* alleles, and we conducted a dual luciferase activity assay. The results showed that TaEIL3 activates the expression of both *TaNPF7.6-A1*^{mod} and *TaNPF7.6-A1*^{lan}; however, there was no significant difference in the relative LUC activity between the two alleles (Fig. 4c, d). Promoter sequences among different alleles are relatively conserved, with only a few SNPs. Together, these results suggest that the differences in the transcriptional levels of *TaNPF7.6-A1*^{mod} and *TaNPF7.6-A1*^{lan} are not due to the promoters, indicating the presence of additional regulatory mechanisms.

To investigate the function of *TaEIL3* in regulating NUE, we generated two *TaEIL3* knockout lines and two *TaEIL3* overexpression lines on the ZM7698 background for further analysis (Supplemental Fig. 13a, b). As expected, under NN and LN hydroponic conditions, the *TaEIL3* overexpression lines exhibited significant growth advantages compared to the wild type (Fig. 4e and Supplemental Fig. 13c-h). We measured the nitrogen content, $^{15}NO_3^-$ influx rate and transport capacity in the *TaEIL3* mutant and overexpression lines of wheat seedlings. We found that *TaEIL3* positively regulates nitrate uptake and transport in wheat (Fig. 4f-i). Significantly increased expression of *TaNPF7.6-A1* was also detected in the *TaEIL3* EO1 and EO2 lines compared to the ZM7698 (Fig. 4j). In a field experiment, the aboveground parts of the EO1 and EO2 lines exhibited more vigorous growth than the wild type, with more developed root systems. Their growth was significantly better than that of the wild type and ec lines (Fig. 4k and Supplemental Fig. 13i-j). Nitrogen accumulation, especially in grains, it increased significantly (Fig. 4l, m). Similarly, the yield per plant of the EO1 and EO2 lines also increased (Fig. 4n). Statistical analysis showed a significant increase in the number of effective spikes, however, the 1000-grain weight, grain number per spike, and the spike length remained unaffected. The opposite was true for ec1 and ec2 (Supplemental fig. 13k-n). In conclusion, our results confirm that TaEIL3 can directly bind to and activate *TaNPF7.6-A1*, thereby regulating its expression level of *TaNPF7.6-A1* and promoting high NUE and yield.

The natural variation in TaNPF7.6-A1 affects the interaction intensity with TaJAZ1 and alters the nucleo-plasmic distribution of TaJAZ1

To further explore the regulatory network of TaNPF7.6-A1 in NUE, we conducted a yeast two-hybrid screen using TaNPF7.6-A1^{mod} as a bait. Considering that the variation of the TaNPF7.6-A1 protein itself might be a key factor influencing the differences in transcriptional levels, and

identified 38 potential proteins that interact with TaNPF7.6-A1^{mod} (Supplemental Data 8). Noteably, a member of the JAZs encoded by TraesCS5A02G204900.1 has attracted particular attention, and was named TaJAZ1 due to its highest percent identity when compared to *Arabidopsis thaliana* sequences[18]. Previous studies have shown that overexpression of *TaJAZ1ΔJas* reduces effective spike number and grain number per spike, while triple homozygous mutants exhibit a significantly increased wheat yield[19,20].

To verify the results of our yeast two-hybrid screening library, we conducted a yeast two-hybrid experiment and a split-LUC assay to confirm TaJAZ1 interact with TaNPF7.6-A1^{mod} or TaNPF7.6-A1^{lan} (Fig. 5a, b). Compared with co-rotating TaJAZ1-nLUC + cLUC-TaNPF7.6-A1^{Lan}, TaJAZ1-nLUC + cLUC-TaNPF7.6-A1^{mod} have more obvious fluorescence signals (Fig. 5c). To confirm these findings in vivo, we conducted a Co-IP assay and a western blotting analysis using Flag and Myc antibodies. This analysis showed that the TaNPF7.6-A1^{mod}-Flag and TaNPF7.6-A1^{lan}-Flag fusion proteins were detected, the TaNPF7.6-A1^{mod}-Flag signal was stronger (Fig. 5d). Subcellular localization analysis revealed that TaJAZ1 was distributed in both the nucleus and the cytoplasm. The fluorescence signal was stronger in the nucleus than in the cytoplasm (Supplemental Fig. 14a, b). The interaction of TaNPF7.6-A1-YFP^{C} and TaJAZ1-YFP^{N} in the cytoplasm was discovered by using BiFC (Fig. 5e). In conclusion, these results indicate that TaJAZ1 interacts with TaNPF7.6-A1 in the cytoplasm. Compared with TaNPF7.6-A1^{lan}, TaJAZ1 interacts more intensely with TaNPF7.6-A1^{mod}.

The interaction strength between the two TaNPF7.6-A1 alleles and TaJAZ1 may alter the subcellular localization of TaJAZ1. Confocal microscopy revealed that, compared to TaJAZ1 and TaNPF7.6-A1^{lan}, TaJAZ1 and TaNPF7.6-A1^{mod} exhibited greater overlap in fluorescence at the cytoplasmic margin (Fig. 5f). Nucleoplasmic separation analysis also indicated that co-

326 expressing TaJAZ1 and TaNPF7.6-A1^{lan}, the abundance of the nuclear localization signal of
327 TaJAZ1 was significantly higher. In contrast, co-expressing TaJAZ1 and TaNPF7.6-A1^{mod},
328 TaJAZ1 abundance of in the cytoplasm was higher (Fig. 5g, h). These results all indicate that
329 TaJAZ1 interacts more strongly with TaNPF7.6-A1^{mod}, leading to increased export of TaJAZ1
330 from the nucleus to the cytoplasm.

331 **TaJAZ1 interferes with the transcriptional regulation of *TaNPF7.6-A1* by TaEIL3 to**
332 **different extents, resulting in expression differences among *TaNPF7.6-A1* alleles**

333 JAZ proteins typically function by forming complexes with other proteins or transcription
334 factors, and indirectly regulating gene expression through interaction with other transcription
335 factors[21]. We found that TaJAZ1 is not directly involved in the regulation of *TaNPF7.6-A1*
336 expression (Supplemental Fig. 14c). In *Arabidopsis thaliana*, it has been reported that
337 EIN3/EIL1 physically interacts with JAZ proteins (JAZ1, JAZ3, and JAZ9), and represses the
338 transcriptional activities of EIN3/EIL1. Removal of the JAZ proteins alleviate this inhibition
339 and promotes root growth[22]. Due to the homology between TaEIL3 and AtEIN3/EIL1
340 (Supplemental Fig. 14d), it is suggested that the JAZ1-EIN3/EIL1 interaction pattern elucidated
341 in *Arabidopsis thaliana* may be conserved in wheat. Therefore, we propose a conjecture that
342 TaJAZ1 interacts with TaEIL3, thereby inhibiting the transcriptional activation of *TaNPF7.6-*
343 *A1* by TaEIL3. The difference in the nuclear localization of TaJAZ1 may interfere with the
344 transcriptional activation of different *TaNPF7.6-A1* alleles by TaEIL3 and leading to the
345 differences in their transcriptional levels. To verify this possibility, we conducted a split-LUC
346 assay and a Co-IP assay determined TaJAZ1 interacts with TaEIL3 (Fig. 6a, b). In the BiFC
347 assay, fluorescence was produced in tobacco leaves co-infected TaJAZ1-YFP^{N} and TaEIL3-
348 YFP^{C}, which were located in the nucleus (Fig. 6c). Collectively, these results demonstrate that

TaJAZ1 interacts with TaEIL3 and occurs in the nucleus.

TaEIL3 can activate the expression of *TaNPF7.6-A1*^{mod} and *TaNPF7.6-A1*^{lan}; however, after co-expression with TaJAZ1, this activation effect is significantly inhibited (Fig. 6d). This result was verified using EMSA, an in vitro DNA binding assay that determine the detect interference of TaJAZ1 on the binding of TaEIL3 to the *TaNPF7.6-A1* FAM-labeled probe (Fig. 6e). This indicates that TaJAZ1 inhibits the binding of TaEIL3 to the *TaNPF7.6-A1* promoter. To examine the differential interference of TaJAZ1 with the transcriptional activation of TaEIL3 in the two alleles of *TaNPF7.6-A1*, we performed a transient expression analysis. No significant difference in LUC activity was observed between the co-expression of TaJAZ1, TaEIL3, and *TaNPF7.6-A1*^{mod}*pro:LUC* or TaJAZ1, TaEIL3, and *TaNPF7.6-A1*^{lan}*pro:LUC*. However, differential activation was observed when TaNPF7.6-A1^{mod} and TaNPF7.6-A1^{lan} were added, respectively (Fig. 6d). These experimental results all indicate that the more interacting TaNPF7.6-A1^{mod} can more effectively “capture” TaJAZ1, thereby more effectively releasing the inhibition of TaEIL3 by TaJAZ1. Ultimately, this leads to TaEIL3 being able to more fully activate the transcription of *TaNPF7.6-A1*^{mod}.

We further generated *tajaz1* mutant lines in the ZM7698 background for functional validation (Supplemental Fig. 14e). In the hydroponic culture experiment under NN and LN conditions, the jc lines hydroponic seedlings showed obvious growth advantages compared with the wild type (Fig. 6f and Supplemental Fig. 14f-k). The nitrogen content, $^{15}NO_3^-$ influx rate, and transport activity were significantly increased (Fig. 6g-j), indicating that TaJAZ1 negatively regulates nitrate uptake and transport in wheat. Simultaneously, significantly increased of *TaNPF7.6-A1* expression was detected in the jc lines compared to the ZM7698 (Fig. 6k). The biomass and grain nitrogen accumulation of the jc lines increased significantly

(Fig. 6l-m and Supplemental Fig. 14l, m), as did the effective spike number and yield per plant. Other agronomic traits changed little (Fig. 6o and Supplemental Fig. 14n-q). In conclusion, these findings suggest that TaJAZ1 interacts with TaEIL3 to negatively regulate wheat NUE, and TaJAZ1 interferes with the transcriptional regulation of *TaNPF7.6-A1* by TaEIL3 to different extents. This results in differences in the expression of the two *TaNPF7.6-A1* alleles.

The breeding potential and geographical distribution of *TaNPF7.6-A1^{mod}*

To further evaluate the breeding potential of *TaNPF7.6-A1^{mod}* for molecular plant breeding, we conducted field plot trials with high planting densities of NILs, ZM7698 and Z-NO2, Fielder and F-NO2. Then, we evaluated their yield performance in NN and LN fields. The GY, NAA and GNA of NIL^{mod} were significantly higher than those of NIL^{lan} (Fig. 7a-d). Compared with ZM7698, the GY, NAA and GNA of Z-NO2 increased significantly increased under different nitrogen treatments over two years. GY increased by an average of 15.11% and 17.15% in the NN fields and by an average of 13.99% and 10.91% on average in the LN fields, respectively (Fig. 7e-h). The yield of F-NO2 increased by an average of 19.50% and 17.77% on average under NN and LN fields, respectively (Supplemental Fig. 15a, b). A significant increase in aboveground nitrogen accumulation was detected in the *TaNPF7.6-A1^{mod}* overexpression lines, especially in the grains (Supplemental Fig. 15c, d). These results indicate that *TaNPF7.6-A1^{mod}* is an elite allele, and that increasing its expression can significantly enhance the NUE and grain yield of wheat plot trials.

We present the geographical distribution of *TaNPF7.6-A1* through allele analysis based on the Watkins & Worldwide Wheat G2B database (https://wwwg2b.com/) of 1007 worldwide wheat accessions[23]. Using 188 modern cultivars and 819 A. E. Watkins landraces, we studied the geographic diversity of *TaNPF7.6-A1* (Supplemental Data 9). The distribution of the two

395 *TaNPF7.6-A1* alleles varies greatly among different varieties. *TaNPF7.6-A1^{mod}* has an
396 overwhelming presence among modern cultivars but is present in only 14.36% among landraces.
397 In contrast, *TaNPF7.6-A1^{lan}* dominates among landraces, and accounts for only 32.60% of
398 modern cultivars (Fig. 7i). This significantly differentiated allele distribution suggests that
399 *TaNPF7.6-A1^{mod}* may be associated with the agronomic traits selected in modern breeding.
400 From a global geographical perspective, *TaNPF7.6-A1^{mod}* shows a distinct regional aggregation.
401 Its high-frequency distribution area is mainly located around Mediterranean (Fig. 7i, j). This
402 indicates that *TaNPF7.6-A1^{mod}* may be a geographically adaptive allele. Interestingly, high
403 frequency distribution area of *TaNPF7.6-A1^{mod}* exhibits a significant spatial overlap with
404 regions of wheat that demonstrate high yield per unit area (Supplemental fig. 15e).

405 To investigate the selection of *TaNPF7.6-A1^{mod}* in wheat breeding in China, 628 modern
406 Chinese cultivars and 177 Chinese landraces were genotyped using CAPS markers. The overall
407 frequency of *TaNPF7.6-A1^{mod}* was found to be 63.11%. However, its distribution among
408 landraces and modern cultivars is extremely uneven. *TaNPF7.6-A1^{lan}* is dominant among
409 landraces, while *TaNPF7.6-A1^{mod}* has become the dominant allele among modern Chinese
410 cultivars (Supplemental Data 10 and Supplemental Fig. 15f, g). From before 1980 to after 2020,
411 the frequency of *TaNPF7.6-A1^{mod}* increased from 22.22% (before 1980) to 57.14% (1981-1990),
412 61.54% (1991-2000), 74.63% (2001-2010), 81.05% (2011-2020) among 628 modern Chinese
413 cultivars. It has remained at high levels since then (Fig. 7k). These results all indicate that
414 *TaNPF7.6-A1^{mod}* has replaced *TaNPF7.6-A1^{lan}* as the absolute dominant allele in modern wheat
415 breeding in China and was strongly positively selected in Chinese wheat breeding.

416 **Discussion**

417 NUE is a complex trait controlled by multiple genes. Yield serves as the direct indicator for

418 assessing NUE under identical nitrogen application levels. However, multiple indicators also
419 need to be considered comprehensively. In this study, we collected 244 wheat germplasms, and
420 performed CGAS and GWAS on a diverse wheat population displaying different NUE-related
421 phenotypes over three consecutive years under NN and LN fields. We mined the same new
422 nitrate transporter *TaNPF7.6-A1* and identified its elite allele *TaNPF7.6-A1*^{mod} (Fig. 1a-c). A
423 series of functional evaluations revealed that transgenic material containing *TaNPF7.6-A1*^{mod}
424 exhibited a "superior" absolute yield under normal nitrogen treatment, and also exhibited a
425 "significantly stronger" growth advantage and yield under low nitrogen treatment (Fig.2 and
426 Supplemental fig. 4). Our study also identified 15 *NPF* genes associated with GNA and NAA
427 (Supplemental Data 2). Among them, eight SNP loci of *NPF* genes were significantly
428 associated with the corresponding NUE phenotypes (Supplemental Data 5). We conducted a
429 gene aggregation analysis on these eight *NPF* genes in 20 varieties with different NUE-related
430 phenotypes and found that the varieties with high NUE, particularly ZM1860, contain the
431 largest number of superior alleles (Fig. 1e and Supplemental Data 6). This indicates the core
432 role of the *NPF* gene family in the efficient nitrogen utilization in wheat. More importantly, it
433 is feasible and efficient to aggregate a large number of superior *NPF* alleles in one genetic
434 background through natural variation or breeding selection. While the effect of a single gene
435 may be limited, but when a variety, like ZM1860, aggregates superior alleles at multiple *NPF*
436 genes, a powerful "cumulative effect" occurs. Although this study focuses on *TaNPF7.6-A1*,
437 this in no way indicates that the remaining *NPF* genes lack research value. Systematically
438 analyzing other *NPF* genes will help us create a comprehensive genetic map of NUE in wheat.
439 Only a few *NPF* genes in wheat, such as *TaNPF2.12* and *TaNPF6.2*, have been reported[13,14].
440 These studies have verified the phenotypes based on transgenic techniques or allele analysis.

441 However, the regulatory and interaction networks of the wheat *NPF* genes have not yet been
442 systematically studied. Our study focused on the newly identified *TaNPF7.6-A1* gene and found
443 that it could be stably expressed at various nitrogen levels (from nitrogen deficiency to
444 sufficiency; Fig.1d), and enhance nitrate uptake by roots, promoting the transport of nitrogen
445 to grains. Ultimately, this increases grain yield and nitrogen use efficiency (Fig. 2, Fig. 3 and
446 Table 1). This differs from the fact that *TaNPF2.12* and *TaNPF6.2*, which are strongly induced
447 by nitrogen signals and function in specific nitrogen environments. Even more unique is the
448 fact that molecular mechanism of its functional advantage differs from that of the reported
449 *OsNPF6.1* in rice[24]. The amino acid mutation of TaNPF7.6-A1^{mod} enhances the transporter
450 activity and has a high transcriptional level in wheat varieties containing *mod* (Fig. 1i and Fig.
451 3c), *OsNPF6.1*^{HapB} is also a transporter with dual advantages in rice. However, we found that
452 the *TaNPF7.6-A1* superior allele is not mainly driven by variations in the promoter, as is the
453 case with *OsNPF6.1*^{HapB} in rice. *OsNPF6.1*^{HapB} enhances its binding to the transcription factor
454 OsNAC42 by acquiring the CACG motif, thereby achieving an expression level advantage in
455 the transcriptional expression[24]. Initially, we also considered whether the transcriptional
456 superiority of *TaNPF7.6-A1*^{mod} originated from a similar mechanism. Therefore, we first
457 conducted a systematic analysis of the promoter sequences of different *TaNPF7.6-A1* alleles.
458 The sequencing results indicated limited variation in the promoter (Supplemental Fig. 11a). To
459 further verify this, we amplified different allele promoters and introduced a new interacting
460 transcription factor, TaEIL3. However, the Dual-LUC assay revealed that there was no
461 significant difference in the activation ability of TaEIL3 for the *mod* or *lan* promoters (Fig. 4c,
462 d). Furthermore, by predicting the binding sites of other potential transcription factors revealed
463 that they were also rarely located in the region of sequence variation (Supplemental Fig. 12).

Through an in-depth analysis of the proteins of different alleles, we found that, although the superior allele TaNPF7.6-A1^{mod} and the inferior allele TaNPF7.6-A1^{lan} are both specifically located on the vacuole membrane (Supplemental Fig. 5c, d). By screening wheat cDNA yeast libraries (DUAL membrane system), we identified a transcriptional inhibitory factor, TaJAZ1. The interaction between TaNPF7.6-A1^{mod} and TaJAZ1 is stronger (Fig. 5a-e), and it regulates the nuclear and cytoplasmic distribution of the transcriptional repressor TaJAZ1 through differential interaction (Fig. 5f-h), This progress reverses the control of its own transcription. The strong-interaction allele TaNPF7.6-A1^{mod} "retains" more TaJAZ1 in the cytoplasm, and relieves its inhibitory function, achieving high expression, and ultimately leading to changes in different allele phenotypes (Fig. 7l). In our research, we verified the function of *TaNPF7.6-A1* and revealed that the functional differentiation of its allele is driven by the intensity of protein-protein interactions rather than promoter sequence variations.

From a global perspective, *TaNPF7.6-A1^{mod}* shows a significant aggregation in the Mediterranean (Fig. 7i-j). This non-random geographical distribution strongly suggests that it has been subject to natural selection. The Mediterranean climate, which features mild, rainy winters and long, hot, and dry summers[25], may have been continuously selected for this allele due to its enhanced adaptability during the flowering period. Field phenotypic observations further support this inference. Materials carrying or overexpressing *mod* (NIL^{mod}, Z-NO2, F-NO2) all exhibited early maturity characteristics (Fig. 2a-b and Supplemental Fig. 4c), which is highly consistent with the adaptive hypothesis that *TaNPF7.6-A1^{mod}* regulates early flowering to avoid summer drought stress. Future research can delve deeper into the molecular genetics and analyze the specific pathways through which *TaNPF7.6-A1^{mod}* regulates flowering time. This will provide a more complete chain of evidence for this hypothesis. Meanwhile, the

Mediterranean is a region with a high frequency of the *TaNPF7.6-A1*^{mod} allele and relatively advanced modern agricultural technology[26]. According to the wheat yield data per unit area from the Food and Agriculture Organization of the United Nations in 2023 (Supplemental Fig. 15e), the *TaNPF7.6-A1*^{mod} allele is highly likely to form a synergistic allele combination with other excellent agronomic traits, such as effective spikes, that have been developed in high-yield wheat regions. This combination supports regional high and stable yields in the modern agricultural systems. Furthermore, historical germplasm analysis indicates that the frequency of *TaNPF7.6-A1*^{mod} increased significantly from 22.22% before 1980 to 81.05% after 2010 (Fig. 7k). Two-year field plot trials further verified the breeding potential of *TaNPF7.6-A1*^{mod}. Overexpression lines exhibited increased nitrogen accumulation and transport to grains, resulting in a significant yield improvement (Fig. 7a-h and Supplemental Fig. 15a-d). This makes *TaNPF7.6-A1*^{mod} a valuable gene resource for driving future molecular design breeding of wheat and cultivating new, high-yield and high-quality varieties.

Methods

Plant materials and growth conditions

Plants used for growth and nitrogen treatments (*Arabidopsis thaliana*, tobacco and wheat) were cultivated in controlled growth chamber at 22℃ ± 2℃, relative humidity between 45%-55%, 130 mmol photons/m^2/s light intensity, and 16-hour light/8-hour dark photoperiod. For protoplast extraction, seedlings were grown in complete darkness until they developed two fully expanded leaves, at which point they were harvested for protoplast isolation.

For phenotypic evaluation used in association analysis, this study selected 244 accessions as core germplasm resources including 135 landraces and 109 modern cultivars in Henan province with the largest wheat planting area in China. All the accessions were planted in three

growing seasons in the Henan Research and Development Center for Modern Agriculture (Yuan yang County, Henan Province; 35°00' N 113°40' E, 77 m a.s.l.). All trials were arranged as a completely randomized block design with three replications. Each plot was consisted of four rows with 2 m in width and 0.23 m spacing between the rows. Seeds were sown at a rate of 130 seeds per square meter. During the maturity stage, single 1 m row sample segments were manually pulled out with roots in each experimental block. The root system was cut off, and the aboveground parts were divided into two parts: straw (leaf sheaths, leaves, stem, cob, glume shell) and grains. After drying to a constant weight, the grain yield per unit area (GY) and the straw dry weight (SDW) were determined respectively, and two rows in each plot were manually harvested to determine the GY. The straw and grain samples of each accession were respectively subjected to coarse crushing and fine crushing treatment, and then the grain nitrogen content (GNC) and straw nitrogen conten (SNC) was determined by an elemental analyzer (Vario Micro Cube, CN model, Elementar, Hanua, Germany). Based on the SDW and GY, formulas (GY × GNC = GNA; SDW × SNC + GNA = NAA) were applied to the calculation of each accession's aboveground nitrogen accumulation amount (NAA) and grain nitrogen accumulation (GNA), and finally used for GWAS and CGAS.

For phenotypic analysis, field trials were carried out during the 2023-2025 growing season at the Henan Research and Development Center for Modern Agriculture (Yuan yang County, Henan Province; 35°00' N 113°40' E, 77 m a.s.l.). NILs, ZM7698, Z-NO lines, z-nc lines, Fielder, F-NO lines and f-nc lines were planted at low density during the 2023-2024 growing season. Each line was planted four rows with 2 m in width and 0.23 m spacing between the rows with three replications. Each row contained 20 seeds. ZM7698, EO lines, ec lines, and jc lines were planted in the same way during the 2024-2025 growing season. Agronomic traits

were investigated, including yield per plant, effective spike number, grain number per spike, 1000-grain weight, plant height, spike length, straw nitrogen accumulation, and grain nitrogen accumulation, were evaluated based on individual plants under single row conditions. In addition, field plot tests were conducted to compare the NUE and yield performance of NILs, ZM7698 and Z-NO2, Fielder and F-NO2 at high planting densities. Those lines were sown at a rate of 260 grains per square meter in a 12 m^2. NILs, ZM7698, and Z-NO2 were investigated for two consecutive years from 2023 to 2025, Fielder and F-NO2 were investigated for one year from 2023 to 2024. Each treatment was replicated five times per field plot.

All field trials were designed with two nitrogen treatment levels: low nitrogen treatment (LN) and normal nitrogen treatment (NN). Nitrogen fertilizer was applied as base fertilizer before sowing and as top dressing during the jointing stage. Scaffolding was set up for tall and easily lodging accessions using steel pipes and bamboo poles to prevent lodging. The rest of the agricultural operations shall be managed in accordance with the conventional field management. The soil in the experimental field was sandy loam moist soil. Before sowing, soil samples in 0-30 cm soil layer were selected for basic soil fertility analysis. The basic fertilities of the tested soil were shown in Supplemental Data 11.

Genome-wide association studies (GWAS) and candidate gene association analysis (CGAS)

A wheat 660KSNP array, consisting of 499,956 SNPs, was used to genotype all 244 accessions[27]. Missing marker sites were imputed using the Beagle v5.2 software[28], and filtering was performed using the Plink v1.9.0 software based on the minor allele frequency (MAF $\geq$ 0.05)[29]. Ultimately, 358,463 SNPs were obtained for GWAS. Principal component analysis (PCA) was carried out using the PLINK software, a phylogenetic tree was constructed through PHYLIP v 3.698, and the phylogenetic tree was visualized using FigTree v1.4.4. LDBlockShow v1.39 was

used for allele map drawing[30]. Linkage disequilibrium (LD) was evaluated using PopLDdecay v3.41[31], and the LD decay distance was defined as the physical distance when r^2 dropped to half of its maximum value (approximately 2 Mb).

Simultaneously, based on previous studies, 331 members of the wheat *NPF* gene family were identified[32]. SNPs were selected within 2 kb flanking the physical positions of each *NPF* gene, and finally 1121 SNPs were screened for CGAS. The Admixture v1.3 software was used to estimate the population structure[33]. The subgroup number K was set as 1-10. The posterior probability q-value of each material in each subgroup was calculated. The q-values of each material in the population belonging to each subgroup represent the Q matrix of the group structure, which was used as a covariate in the GWAS and CGAS. The 3VmrMLM method was used to conduct the association analysis[34]. The Q matrix was used to control the population structure, and the kinship matrix was calculated by the software. The threshold for significant loci was set as LOD ≥ 3. The Manhattan plot was drawn using R v4.4.2, when the LOD of the corresponding locus was ≥10, the obtained LOD was converted to LOD' = 10+(LOD–10)/5 for display.

Vector construction and plant transformation

For *TaNPF7.6-A1*^{mod} and *TaEIL3*, the complete gene coding sequences (CDSs) without stop codons were amplified using cDNA from ZM1860 7-day-old seedlings and cloned them into vector pWMB110 under, respectively, and created the *Ubi: TaNPF7.6-A1* and *Ubi: TaEIL3* constructs. The resulting vectors containing the desired inserts were transformed into *Agrobacterium tumefaciens* strain EHA105. ZM7698 and Fielder were used as wheat recipient cultivars for *TaNPF7.6-A1*, while ZM7698 was used as the wheat recipient cultivar for *TaEIL3*. For the T_0, T_1, and T_2 generations, T_3 homozygous lines were obtained through PCR

amplification, sanger sequencing, and RT–qPCR expression analysis for field phenotypic evaluation. All primers used are listed in Supplementary Data 12.

To generate mutants of *TaNPF7.6-A1*, *TaEIL3*, or *TaJAZ1* through CRISPR-Cas9, respectively, we designed sgRNA sequences of these genes into the pBUE411 vector. *TaNPF7.6-A1* sgRNA sequence is 5′- CCGCCGCATGTGAAGGAACTTCA-3′, *TaEIL3* sgRNA sequence is 5′- GGATGTGGAAAGATAAGGTCAGG-3′, and TaJAZ1 sgRNA sequence is 5′- CCCCAAGCAGCAGGCCTCCCGCG-3′. These sequences are strictly conserved among the A, B, and D homoeologous genes. ZM7698 and Fielder were used as wheat recipient cultivars for *TaNPF7.6-A1*, while ZM7698 was used as wheat recipient cultivar for *TaEIL3* and *TaJAZ1*. Transgenic plants were also obtained through *Agrobacterium tumefaciens* EHA105-mediated transformation. Homozygous mutants were obtained by PCR amplification and sanger sequencing for field experiments. Primers used are listed in Supplementary Data 12.

TaNPF7.6-A1pro: GUS was constructed in the pBWA(V)BII vector using the complete *TaNPF7.6-A1* gene promoter (the ~2000 bp upstream of the ATG of *TaNPF7.6-A1* CDS), and then transformed into *Arabidopsis thaliana* (Col-0 background). The T_3 homozygous lines were harvested for further research. Primers used are listed in Supplementary Data 12.

RNA sequencing

For RNA-seq, ZM7698 seedlings were grown in wheat nutrient liquid culture containing different nitrate (0 mM, 0.2 mM, 1 mM, 2 mM) for 2 weeks. The specific components of the nutrient solution (pH 5.5-5.8) are shown in Supplementary Data 14. Total RNA was extracted from the shoots and roots, and messenger RNA (mRNA) sequencing libraries were constructed with three biological replicates for each sample.

Sequencing was performed on the NovaSeq high-throughput sequencing platform (Guangzhou Gene Denovo Biotechnology Co., Ltd., Guangzhou, China). Quality control was carried out using fastp[35] to filter out low-quality data. The HISA2 software[36] was used to conduct alignment analysis based on the wheat reference genome (IWGSC RefSeq v2.1). According to the alignment results, Stringtie[37] was used to reconstruct transcripts, and RSEM[38] was used to calculate the expression levels of all genes in each sample. Transcript abundance (gene expression level) was calculated in units of transcripts per million (TPM). Differential gene expression was analyzed using the edgeR software[39]. Genes with an absolute value of log2(fold change) ≥ 1 and a false discovery rate (FDR) < 0.05 were considered differentially expressed.

^{15}N-Nitrate Uptake Assay in *Xenopus laevis* Oocytes

For *TaNPF7.6-A1^{lan}*, the complete gene coding sequence (CDS) without stop codon was amplified using cDNA from Ermangmai 7-day-old seedlings. The CDS of *TaNPF7.6-A1^{mod}* and *TaNPF7.6-A1^{lan}* was amplified and cloned into the pGEMHE-mCherry vector between the restriction sites *Xma* I and *Eco* RI, and then was linearized by *Nhe* I, as previously reported[40]. The linearized vector was recovered from the digested products using a DNA purification kit (QIAGEN, 28304). Using the linearized vector as a template, cRNA was obtained by transcription with a mMESSAGE mMACHINE^{TM} T7 Transcription kit (Invitrogen, AM1344). The DNA template was digested with DNaseI provided in the kit, and the cRNA was purified by the LiCl method to remove salts, dissolved in H_2O (Nuclease-free), and its concentration was adjusted to 1-1.5 μg/μl using a Nano-Drop. *Xenopus laevis* Oocytes were obtained, and the envelopes on the oocyte surface were removed by enzymatic digestion with 30 mg/ml collagenase D (Roche, 11088858001) at 22°C for 2 h. Mature oocytes at stage IV-VI were

selected, and cRNA was injected using a microinjection system. After injection, the oocytes were incubated in Ringer's solution at 16℃ for 36 h. Dead oocytes were promptly removed, and the fresh solution was replaced. Fluorescence was detected using fluorescence confocal microscope, Leica SP8 Laser confocal microscope (Leica, GER), and mCherry fluorescence was excited with a 546 nm laser. Then, the normally luminescent oocytes were transferred to ND96 containing 0.25 mM $K^{15}NO_3$ or 10 mM $K^{15}NO_3$ and incubated for 10 h for ^{15}N-nitrate uptake analysis. The formulation of ND96 was 0.25 mM/10 mM $K^{15}NO_3$ (98%atom $K^{15}NO_3$, Sigma-Aldrich, 335134), 230 mM Mannitol, 0.3 mM $CaCl_2$, 10 mM MES-Tris, pH 5.5 or 7.5. For each sample, one oocyte was analyzed as an independent sample, and 11 repeated replicates at least were conducted. The experiment set injection of the same volume of water as the negative control and *AtNRT1.1* as the positive control. After the oocytes were dried to a constant weight at 65°C, the $\delta^{15}N/^{14}N$ ‰ of each oocyte was determined by the SData Isotope Ratio Mass Spectrometry (Flash EA-DELTA V Advantage, USA), the methods were performed as previously described[41]. Primers used are listed in Supplementary Data 12.

Subcellular localization

For subcellular localization assays, the CDS of *TaNPF7.6-A1*^{mod}, *TaNPF7.6-A1*^{lan}, *TaEIL3* and *TaJAZ1* without stop codons, were cloned into the pAN580 vector digested by *Xba* I and *Bam* HI to generate GFP fusion constructs, respectively. These constructs were then transformed into wheat protoplasts for analysis. Wheat protoplasts were incubated in the dark at 24℃ for 14-16 h. Meanwhile, the same CDSs without stop codons were also inserted into 1305-GFP or 1305-mCherry digested by *Xba* I and *Bam* HI, and then introduced into the tobacco leaves by using *Agrobacterium tumefaciens* GV3101-mediated transformation for 48 h. Fluorescence signals were visualized by Nikon confocal laser scanning microscope (C2-ER, Japan). The primers

used are listed in Supplementary Data 12.

RNA extraction and RT–PCR

Total RNA was extracted from different tissues of wheat using the Plant RNA Purification Kit (Monad, MI20201S), first-strand cDNAs were synthesized from 1 μg of total RNA using the HiScript reverse transcription Kit (Vazyme, R323) according to the instructions of manufacturer. For RT-qPCR, the reaction mixture consisted of 2 μl of cDNA template, 0.8 mM primers, and 10 μl of 2×ChamQ Universal SYBR qPCR Master Mix (Vazyme, Q711) in a final volume of 20 μl. Amplification was performed using a CFX96 real-time system (Bio-Rad, USA). Differences in relative transcript levels were calculated using the 2-ΔCT method relative to wheat *Taα-tubilin*. At least three independent biological duplicate samples were collected for each experiment, all primer sequences are listed in Supplementary Data 12.

GUS staining

To cultivate *TaNPF7.6-A1*^{mod}*pro: GUS Arabidopsis* seedlings, the seeds were first sterilized and then sown on a modified 1/2 MS medium for 7 days, with 2 mM NH_4Cl or 2 mM KNO_3 as the sole nitrogen source[42]. The determination of β-glucuronidase (GUS) activities were carried out using the method described as previously reported[43] with corresponding adjustments. Immediately immerse the 7-day-old seedlings into GUS staining solution containing 1 mM 5-bromo-4-chloro-3-indolyl-β-D-glucuronic acid (X-Gluc, Thermo Scientific, R0851), 100 mM sodium phosphate buffer (pH 7.0), 10 mM EDTA, 2 mM $K_3Fe(CN)_6$, 2 mM K_4 $[Fe(CN)_6]$ and 0.1% (volume ratio) Triton X-100 after harvesting. To enhance the dye penetration, the samples were briefly vacuum impregnated (0.6 Mpa, 10 minutes), and then incubated in the dark at 37°C for 24 hours. After staining, the tissues were washed with gradient ethanol (20%, 50%, and 70% ethanol, each for 1 hour) to remove chlorophyll and background pigments. Histological analysis

671 was observed using a Leica stereoscopic microscope (M205 FA, Germany), and blue
672 precipitates indicated the presence of GUS activity.

673 **Hydroponic culture**

674 Wheat seeds were treated with 5%H_2O_2 for 15 minutes, then soaked overnight at 4℃ in 1%
675 sodium hypochlorite (NaClO). The next day, the seeds were washed with water until there was
676 no sodium hypochlorite smell. Finally, they were soaked in clean water at room temperature till
677 the seeds germinate, with the water changed every 12 hours. Uniformly germinated seeds are
678 selected and put into hydroponic plate, then transferred to clear water until roots length reach 5
679 cm. After removing endosperms, the seedlings were transplanted into black plastic boxes
680 containing 1 L of nutrient solution. The culture solution used for hydroponic culture
681 experiments contained $Ca(NO_3)_2$ (1 mM for normal N treatment and 0.1 mM for low N
682 treatment, respectively).The composition are shown in Supplementary Data 13. The nutrient
683 solution was refreshed every day. Before refreshing, its pH was adjusted to 5.8 with dilute HCl
684 and KOH.

685 Hydroponic experiments were conducted in a controlled growth chamber: the temperature
686 was maintained at 22℃ ± 2℃, relative humidity between 45% - 55%, 130 mmol photons/m^2/s
687 light intensity, and 16-hour light/8-hour dark photoperiod. After 14 days, morphological
688 parameters and plant N concentrations of 15 randomly selected plants were measured, and root
689 morphological analyses were conducted via computerized scanning using Delta-T Scan (Delta-
690 T Devices Ltd., UK) and WinRHIZO (Regent Instrument Inc., Ottawa, Canada). For each
691 sample, the collected seedlings were dried to a constant weight and then crushed. The nitrogen
692 content in the shoots and roots was determined using the Dumas analyzer (Beijing Nord
693 DN3000, China). For each sample, 15 seedlings were collected as samples and 5 biological

694 replicates were used.

695 **^{15}N-Nitrate uptake and translocation assay**

696 The wheat seedlings were cultivated in wheat nutrient solution for 7 days. Then, 1 mM or 0.1
697 mM $Ca(NO_3)_2$ were replaced with 2 mM or 0.2 mM KNO_3, and the cultivation was continued
698 for one week. The previously methods were adopted for the determination of ^{5}N-NO_3^-
699 absorption and transport[44]. All plants were first cultured in a nutrient solution without nitrogen
700 for 3 days before $^{15}NO_3^-$ treatment, and then transferred to wheat nutrient solution containing
701 0.2 or 2 mM ^{15}N-KNO_3 (10% atom $K^{15}NO_3$, Sigma-Aldrich, 348481). After 3 h absorption,
702 wheat roots are rinsed with 0.1 mM $CaSO_4$ for 2 min to remove the ^{15}N-KNO_3, the roots and
703 shoots were harvested respectively, dried in an oven at 70°C for 72 hours, and then the dry
704 weight was measured. Finally, the samples were ground and determined by isotope ratio mass
705 spectrometer (Finnigan Delta Plus XP, Thermo Fisher Scientific, USA) with an elemental
706 analyzer (Flash EA 1112, Thermo Fisher Scientific, USA). About 0.5 mg dried powder is
707 analyzed by isotope ratio mass spectrometer and the data of ^{15}N content are obtained. While
708 detecting the ^{15}N-nitrate uptake activity, a formula (total ^{15}N amount of whole plant /dry weight
709 of root /3 h) is applied to the calculation, the amount of ^{15}N take up per unit weight of roots per
710 unit time, total ^{15}N amount of whole plant is derived from the sum of N amount of shoots and
711 roots. The ratio of shoot ^{15}N content to root ^{15}N content is used to represent the root-to-shoot
712 transport activity, the higher the value, the higher root to shoot transport activity. For each
713 sample, 15 seedlings were collected as samples and 5 biological replicates were used.

714 **Protein-DNA interactions predicted by AlphaFold3**

715 The amino acid sequences of 3397 wheat transcription factors were collected. The three-
716 dimensional (3D) structure of each sequence was constructed using AlphaFold3[16]. The 3D

structure of the *TaNPF7.6-A1* promoter (2000 bp sequence upstream of transcription start codon, ATG) was constructed using 3DNA[45]. After completion, the 3D structure of the *TaNPF7.6-A1* promoter was sequentially aligned with the 3D structure of each transcription factor amino acid sequence by using megadock software[17]. After the analysis is completed, the 3D modeling score of the transcription factor amino acid and the interaction score will be obtained. Details are provided in Supplementary Data 7. If the 3D structure modeling score reaches over 100%, we can consider that the prediction model fully represents the true result. The interaction score is the predicted score obtained by docking the *TaNPF7.6-A1* promoter with the transcription factor amino acid sequence. Among them, *p53* and pGADT7-p53m were positive control.

Yeast one-hybrid assay (Y1H)

The promoter fragments of *TaNPF7.6-A1*^{mod}, *TaNPF7.6-A1*^{lan}, P1, P2 and P3 were amplified from ZM1860 and Ermangmai 7-day-old seedlings genomic DNA, respectively, and cloned into the pAbAi vector digested by *Kpn* I and *Sal* I. The constructs were linearized through *Bst* BI digestion and transformed into Y1HGold cells to generate bait strains. Insert the CDS of *TaEIL3* into pGADT7 to transform the Y1H bait strains. The transformants were selected on a synthetic dropout medium lacking Ura and Leu and supplemented with 600 ng/ml AbA. Primers used are listed in Supplementary Data 12.

Electrophoretic mobility shift assay (EMSA)

Electrophoretic mobility shift assay (EMSA) was carried out in accordance with the methods described before[46]. The CDS of *TaEIL3* was inserted into the vector pGEX-4T-1 digested by *Bam* HI and *Eco* RI, and the CDS of *TaJAZ1* was inserted into the vector pET-32a (+) by *MSC* I and *SalI* I and all expressed in *E. coli* Rosetta (DE3). The recombinant protein was purified on glutathione Sepharose 4B (GE Healthcare, 17075601) or Ni-NTA Agarose (Qiagen, 30230)

according to the manufacturer's instructions. The DNA fragments were labeled at the 5' end with 5'-carboxylfluorescein (FAM). The labeled DNA probe was combined with purified GST, GST- TaEIL3, or TaJAZ1-His in a 20μL binding buffer containing 50 mM Tris-HCl (pH 7.5), 5 mM EDTA, 10 mM $MgCl_2$, 0.5 M NaCl, 5mM DTT, 0.05 mg/mL poly (dI-dC) and 4% (v/v) glycerol at 25°C for 30 minutes. The unlabeled competitive DNA probes were also added to the competition assays. The reaction mixtures were electrophoresed at 4 °C on a 6 % native polyacrylamide gel in 0.5×TBE buffer for 60-90 min at 150 V, and imaged on a Typhoon 9400 imager (GE Healthcare, USA). Primers used are listed in Supplementary Data 12.

Bimolecular fluorescence complimentary assay (BiFC)

In the BiFC assay, the full-length coding sequence of *TaJAZ1* was amplified and cloned into the pSPYNE vector digested with *Bam* HI and *Xba* I, while the full-length coding sequences of *TaEIL3*, *TaNPF7.6-A1*^{mod} and *TaNPF7.6-A1*^{lan} were amplified and cloned into the pSPYCE vector digested with *Bam* HI and *Xba* I, respectively, and then transformed into *Agrobacterium* strain GV3101. The transformed cells were cultured in 10 ml LB liquid medium containing kanamycin and rifampicin until OD600 reached 1.5. The transformed bacteria were collected by centrifugation and resuspended in osmotic buffer (10mM MES, 10 mM $MgCl_2$ and 0.2 mM acetosyringone) with a final concentration of OD600 = 1, and let them stand in the dark for 2 h. Appropriate combinations were mixed and co-infiltrated them into the tobacco leaves. After 48 h, the fluorescence signals were detected using a Nikon confocal laser scanning microscope (Nikon, C2-ER). Primers used are listed in Supplementary Data 12.

Dual-luciferase reporter assay (Dual-LUC)

The promoter sequences of *TaNPF7.6-A1*^{mod} and *TaNPF7.6-A1*^{lan} were cloned into the pGreenII0800-LUC vector digested with *Kpn* I and *Bam* HI to generate reporter constructs. The

full-length coding sequences of TaEIL3 and TaJAZ1 were cloned into the pSuper-Myc vector digested with *Xba* I and *Kpn* I as effectors, and GFP was cloned into the pSuper-Myc vector as a control. The different construct combinations were co-expressed in tobacco leaves and cultured for 48 hours. Those leaves' surfaces were treated with D-luciferin (Yeasen, 40902ES01). After two minutes in the dark, LUC signals were observed using a plant in vivo imaging system. Subsequently, the leaves at the injection site were collected and the LUC/REN activities were determined using Dual-Luciferase Reporter Gene Assay Kit (Yeasen, 11402ES80). Primers used are listed in Supplementary Data 12.

The split-ubiquitin yeast system (DUAL membrane)

The DUAL membrane system was used in accordance with the manufacturer's protocols. The prey vectors pPR3-N or pPR3-N-TaJAZ1 (vector pPR3-N digested with *Bam* HI and *Eco* RI) and the bait vectors pBT3-STE, pBT3-STE- TaNPF7.6-A1^{mod} or TaNPF7.6-A1^{lan} (vector pBT3-STE digested by *sfi* I) were co-transformed into the yeast strain NMY51. Yeast cells were spread on SD/-Trp-Leu agar plates and incubated at 29°C for 3 days after transformation. Colonies grown on SD/-Trp-Leu plates were suspended in SD/-Trp-Leu liquid medium to an optical density of 600 (OD600) were 0.6. A 10×dilution series of 10 μl aliquots of co-transformed NMY51 were spotted onto SD/- Trp- Leu and SD/- Leu- Trp- His- Ade agar plates, followed by the examination of LacZ reporter gene with X-Gal as a substrate. Plates were incubated at 29°C for 3 days.

Luciferase complementation imaging assay (LCI)

For the split-luciferase assay, the indicated genes were respectively fused to the pCAMBIA1300-nLUC (nLUC) vector or pCAMBIA1300-cLUC (cLUC) vectors digested with *Kpn* I and *Sal* I. The constructs were transformed into *Agrobacterium* strain GV3101.

Appropriate combinations were mixed and co-infiltrated into the tobacco leaves. Plants were grown under long day (16h light/8h dark) condition for 2 days. Then the leaves were treated with D-luciferin (Yeasen, 40902ES01) and incubated in the dark for two minutes, LUC signals were observed using a plant in vivo imaging system. Primers used are listed in Supplementary Data 12.

Co-Immunoprecipitation assay (Co-IP)

For the Co-IP assay, the full-length coding sequences of each gene shown were cloned into the pSuper-Flag or pSuper-Myc vectors digested by *Xba* I and *Kpn* I, respectively. Each construct was transformed into *Agrobacterium* strain GV3101. Through infection, they were mixed in appropriate combinations and injected into the tobacco leaves. The leaves were harvested after 48 h and proteins were extracted using lysis buffer. The compositions of lysis buffer were: 50 mM Tris-HCl (pH 7.5), 150 mM NaCl, 1 mM EDTA, 10% glycerol, 0.1% NP-40, 1 mM PSMF, 5 mM DTT and 1% protease inhibitor cocktail. The total proteins isolated from different permeable leaves were incubated with anti-Flag magnetic beads at 4°C for 4 to 6 h with gentle rotation. Then wash the magnetic beads four times with PBS containing 0.01% (v/v) Triton X-100. The washed beads were resuspended with 60μL PBS and added with 20μL 4×Protein SDS PAGE Loading Buffe (TaKaRa, 9173). The mixture was boiled for 10 min, then cooled to room temperature and separated in 10% SDS-PAGE gel. The separated proteins were subjected to immunoblotting analysis with anti-Myc (Abmart, M20002) or anti-Flag (Abmart, M20008) antibodies.

Enrichment and detection of nuclear and cytoplasm fractions

The full-length coding sequences of *TaJAZ1*, *TaNPF7.6-A1*^{mod} or *TaNPF7.6-A1*^{lan} were cloned into pSuper-Flag or pSuper-Myc vectors digested with *Xba* I and *Kpn* I, respectively. The

809 primers used are listed in Supplementary Data 13. Each construct was transformed into
810 *Agrobacterium* strain GV3101, then the *Agrobacterium* cultures mixed in appropriate
811 combinations and co-infiltrated into *N. benthamiana* leaves. After 48 h, the proteins of 2 g fresh-
812 weight leaves in each combination were ground in liquid nitrogen and resuspended in 4 mL
813 Honda buffer (25 mM Tris-HCl [pH7.4], 10 mM $MgCl_2$, 2.5% [wt/vol] Ficoll 400 [Sigma,
814 F4375], 5% [wt/vol] Dextran T40 [GE Healthcare, 17-0270-01], 0.4 M sucrose, 1×Protease
815 Inhibitor Cocktai [Roche, 11836145001], 5 mM DTT [Coolabe, CD4941], 50μM MG132
816 [Sigma-Aldrich, M7449]). Then the mixture was incubated on ice for 10 min. The mixture was
817 filtered through magic filter cloth (Merck Millipore, 475855-1R). Triton X-100 was added to a
818 final concentration of 0.5%, and the mixture was incubated on ice for 15 min. The solution was
819 centrifuged at 1500 g for 5 minutes at 4 °C. The supernatant was then transferred to a new tube,
820 while the pellet was placed on ice for later use. Following this, the supernatant underwent two
821 additional rounds of centrifugation. The resulting supernatant was the cytoplasmic component
822 protein (nuclei-depleted fraction) with the nucleus removed. The pellet was resuspended and
823 washed with Honda buffer added with 0.1% Triton X-100, then centrifuged at 1500 g for 5 min
824 and washed 5 times until the washed Honda buffer was completely clear and the pellet was
825 white. Then dissolve the white pellet in 100 μL Honda buffer, which is the nuclei-enriched
826 fraction.

827 Equal amounts of proteins from each sample were mixed with 4×Protein SDS PAGE
828 Loading Buffe (TaKaRa, 9173), and boiled for 10 min. The cytoplasmic components and
829 nuclear components were separated through SDS-PAGE gel and transferred onto nitrocellulose
830 (NC) membrane. The following antibodies were used for western blots to detect those proteins:
831 anti-Flag (Abmart, M20008, 1:10000) and anti-Myc (Abmart, M20002, 1:10000). Meanwhile,

the purity of the extracted nuclear components and cytoplasmic components were determined by detecting the expression levels of Histone H3 antibody (Beyotime, AH433, 1:5000) and Actin antibodies (Zomanbio, ZN101A-1, 1:5000). Cytoplasmic component-specific Actin antibodies demonstrate a strong signal for Actin protein in the cytoplasmic component, while exhibiting a very weak signal in the nuclear component. In contrast, the nuclear component-specific Histone H3 antibody is expected to show robust signaling exclusively in the nuclear component, with no detecData signal in the cytoplasmic component.

Quantification and statistical analysis

P values and sample sizes (n) are indicated in the individual figures and figure legends. Statistical analyses were performed using SPSS v22 (IBM Corp. Armonk, NY, USA) software. A two-tailed Student's *t* test was used to assess differences between two groups, while one-way ANOVA with Duncan's new multiple range test was applied to evaluate differences among multiple groups. Data visualization were performed using GraphPad Prism 8.

Reporting summary

Further information on research design is available in the Nature Portfolio Reporting Summary linked to this article.

Data availability

The genomic information and sequences were downloaded from EnsemblPlants IWGSC Database (https://plants.ensembl.org/Triticum_aestivum/Info/Index) and WheatOmics (http://wheatomics.sdau.edu.cn/). The raw sequence data reported in this paper have been deposited in the Genome Sequence Archive (Genomics, Proteomics & Bioinformatics 2025) in National Genomics Data Center (Nucleic Acids Res 2025), China National Center for Bioinformation (CNCB) (GSA: CRA037933 with BioProject: PRJCA057114), and are publicly

accessible at https://ngdc.cncb.ac.cn/gsa/browse/CRA037933. The variation data reported in this paper have been deposited in the Genome Variation Map (GVM) in CNCB (GVM: GVM001307 with BioProject: PRJCA057114), and are publicly accessible at https://bigd.big.ac.cn/gvm/getProjectDetail?Project=GVM001307. Source data are provided with this paper.

References

1. Canfield, D. E., Glazer, A. N., and Falkowski, P. G. (2010). The evolution and future of Earth's nitrogen cycle. *Science*. **330**: 192-196.
2. Xu, G., Fan, X., and Miller, A. J. (2012). Plant nitrogen assimilation and use efficiency. *Annu Rev Plant Biol*. **63**: 153-182.
3. Hu, B., Wang, W., Chen, J., Liu, Y., and Chu, C. (2023). Genetic improvement toward nitrogen-use efficiency in rice: Lessons and perspectives. *Mol Plant*. **16**: 64-74.
4. Moll, R. H., Kamprath, E. J., and Jackson, W. A. (1982). Analysis and Interpretation of Factors Which Contribute to Efficiency of Nitrogen Utilization1. *Agronomy Journal*. **74**, 562-564.
5. Du, D., Li, Z., Jiang Z., Yuan, J., Zhang, X., Zhao, H., Tian, L., Liu, Y., Li, R., He, F., et al. (2025). The Transcription Factor WFZP Interacts with the Chromatin Remodeler TaSYD to Regulate Root Architecture and Nitrogen Uptake Efficiency in Wheat. *Adv Sci (Weinh)*. **12**: e2416433.
6. Xu W., Chen Y., Niu Y., Liu B., Du D., Ning X., Huan T., Zhou Y., Ke W., Miao L., et al. (2025). An incoherent feed-forward loop coordinates nitrate uptake and tillering in wheat. *Mol Plant*. **18**: 1881-1900.
7. Li, Z., Na, Wu. X., Jacquot, A., Chaput, V., Adamo, M., Neuhäuser, B., Straub, T., Lejay, L., Schulze, WX. (2024). Phosphoregulation in the N-terminus of NRT2.1 affects nitrate uptake by controlling the interaction of NRT2.1 with NAR2.1 and kinase HPCAL1 in *Arabidopsis*. *J Exp Bot*. **75**: 2127-2142.
8. Meng, X., Lou, H., Zhai, S., Zhang, R., Liu, G., Xu, W., Yu, J., Zhang, Y., Ni, Z., Sun, Q.,

et al. (2024). *TaNAM-6A* is essential for nitrogen remobilisation and regulates grain protein content in wheat (Triticum aestivum L.). *Plant Cell Environ*. **47**: 2310-2321.

9. Wang, Y., Zhang, Y., An, Y., Wu, J., He, S., Sun, L., and Hao, F. (2022). Wheat *TaTIP4;1* confers enhanced tolerance to drought, salt and osmotic stress in *Arabidopsis* and rice. *Int J Mol Sci*. **23**: 2085.
10. Sadras, V. O., Hayman, P. T., Rodriguez, D., Monjardino, M., Bielich, M., Unkovich, M., Mudge, B., Wang, E. (2016). Interactions between water and nitrogen in Australian cropping systems: physiological, agronomic, economic, breeding and modelling perspectives. *Crop and Pasture Science*. **67**: 1019-1053.
11. Anne, K., David, L. C., Camille, C., Thomas, G., Anne, M., Anne-Sophie, L., Sylvain, C., Sylvie, F., Christian, M., Françoise, D. (2014). Nitrate transport and signalling in *Arabidopsis*. *J Exp Bot*. **65**: 789-798.
12. Li, M., Tian, H., and Gao, Y. (2021). A genome-wide analysis of *NPF* and *NRT2* transporter gene families in bread wheat provides new insights into the distribution, function, regulation and evolution of nitrate transporters. *Plant and Soil*. **465**: 47-63.
13. Wang, H., Liu, Y., Wu, L., Xia, C., Chen, Y., Kong, X., Shi, F., Li, H., Yang, X., Ma, L., et al. (2025). *TaNPF6.2* improves agronomic traits via enhancing nitrogen uptake efficiency in wheat. *J Genet Genomics*. **52**: 120-123.
14. Siddiqui, MN., Pandey, K., Bhadhury, SK., Sadeqi, B., Schneider, M., Sanchez-Garcia, M., Stich, B., Schaaf, G., Léon, J., Ballvora, A. (2023). Convergently selected *NPF2.12* coordinates root growth and nitrogen use efficiency in wheat and barley. *New Phytol*. **238**: 2175-2193.
15. Wolfenstetter, S., Wirsching, P., Dotzauer, D., Schneider, S., and Sauer, N. (2012). Routes to the tonoplast: the sorting of tonoplast transporters in Arabidopsis mesophyll protoplasts. *Plant Cell*. **24**: 215-232.
16. Jumper, J., Evans, R., Pritzel, A., Green, T., Figurnov, M., Ronneberger, O., Tunyasuvunakool, K., Bates, R., Žídek, A., Potapenko, A., et al. (2021). Highly accurate protein structure prediction with AlphaFold. *Nature*. **596**: 583-589.
17. Ohue, M., Shimoda, T., Suzuki, S., Matsuzaki, Y., Ishida, T., and Akiyama, Y. (2014). MEGADOCK 4.0: an ultra-high-performance protein-protein docking software for heterogeneous supercomputers. *Bioinformatics*. **30**: 3281-3283.

18. Ju, L., Jing, Y., Shi, P., Liu, J., Chen, J., Yan, J., Chu, J., Chen, KM., and Sun, J. (2019). JAZ proteins modulate seed germination through interaction with ABI5 in bread wheat and Arabidopsis. *New Phytol*. **223**: 246-260.
19. Ye, B., Liu, Y., Wang, Z., Shen, L., Yin, C., Shen, K., Sun, J., Xu, X., Sun, M., Wu, J., et al. (2024). Genetic basis of geographical differentiation, breeding selection, domestication effects, and breeding application for *TaJAZ1* in wheat. *J Genet Genomics*. **51**: 665-668.
20. Yuan, S., Zhang, D., Xiao, Y., Wang, X., Liu, H., Wang, J., Zhang, H., Kang, G., Li, G. (2025). TaJAZ1-mediated transcriptional regulation of starch biosynthesis synergistically enhances resistant starch content and yield in wheat. *The Crop Journal*. **13**: 1731-1745.
21. Zhao, X., He, Y., Liu, Y., Wang, Z., and Zhao, J. (2024). JAZ proteins: Key regulators of plant growth and stress response. *The Crop Journal*. **12**: 1505-1516.
22. Zhu, Z., An, F., Feng, Y., Li, P., Xue, L., A, M., Jiang, Z., Kim, JM., To, TK., Li, W., et al. (2011). Derepression of ethylene-stabilized transcription factors (EIN3/EIL1) mediates jasmonate and ethylene signaling synergy in *Arabidopsis*. *Proc Natl Acad Sci U S A*. **108**: 12539-12544.
23. Cheng, S., Feng, C., Wingen, LU., Cheng, H., Riche, AB., Jiang, M., Leverington-Waite M, Huang Z., Collier, S., Orford, S., et al. (2024). Harnessing landrace diversity empowers wheat breeding. *Nature*. **632**: 823-831.
24. Tang, W., Ye, J., Yao, X., Zhao, P., Xuan, W., Tian, Y., Zhang, Y., Xu, S., An, H., Chen, G., et al. (2019). Genome-wide associated study identifies NAC42-activated nitrate transporter conferring high nitrogen use efficiency in rice. *Nat Commun*. **10**: 5279.
25. Dakroub, H., Sgroi, G., D'Alessio, N., Russo, D., Serra, F., Veneziano, V., Rea, S., Pucciarelli, A., Lucibelli, MG., et al. (2023). Molecular Survey of Toxoplasma gondii in Wild Mammals of Southern Italy. *Pathogens*. **12**: 471.
26. Molénat, J., Barkaoui, K., Benyoussef, S., Mekki, I., Zitouna, R., and Frédéric, J. (2023). Diversification from field to landscape to adapt Mediterranean rainfed agriculture to water scarcity in climate change context. *Current Opinion in Environmental Sustainability*. **65**: 101336.
27. Zhang, Z., Peng, C., Xu, W., Li, Y., Qi, X., and Zhao, M. (2024b). Genome-wide association study of agronomic traits related to nitrogen use efficiency in Henan wheat. *BMC Genomics*. **25**: 7.

28. Browning, B. L., Tian, X., Zhou, Y., and Browning, S. R. (2021). Fast two-stage phasing of large-scale sequence data. *Am J Hum Genet*. **108**: 1880-1890.
29. Chang, C. C., Chow, C. C., Tellier, L. C., Vattikuti, S., Purcell, S. M., and Lee, J. J. (2015). Second-generation PLINK: rising to the challenge of larger and richer datasets. *Gigascience*. **4**: s13742-015-0047-8.
30. Dong, S. S., He, W. M., Ji, J. J., Zhang, C., Guo, Y., and Yang, T. L. (2021). LDBlockShow: a fast and convenient tool for visualizing linkage disequilibrium and haplotype blocks based on variant call format files. *Brief Bioinform*. **22**: bbaa227.
31. Zhang, C., Dong, S. S., Xu, J. Y., He, W. M., and Yang, T. L. (2019). PopLDdecay: a fast and effective tool for linkage disequilibrium decay analysis based on variant call format files. *Bioinformatics*. **35**: 1786-1788.
32. Wang, H., Wan, Y., Buchner, P., King, R., Ma, H., and Hawkesford, M. J. (2020). Phylogeny and gene expression of the complete NITRATE TRANSPORTER 1/PEPTIDE TRANSPORTER FAMILY in Triticum aestivum. *J Exp Bot*. **71**: 4531-4546.
33. Alexander, D. H., Novembre, J., and Lange, K. (2009). Fast model-based estimation of ancestry in unrelated individuals. *Genome Res*. **19**: 1655-1664.
34. Li, M., Zhang, YW., Zhang, ZC., Xiang, Y., Liu, MH., Zhou, YH., Zuo, JF., Zhang, HQ., Chen, Y., Zhang, YM. (2022b). A compressed variance component mixed model for detecting QTNs and QTN-by-environment and QTN-by-QTN interactions in genome-wide association studies. *Mol Plant*. **15**: 630-650.
35. Chen, S., Zhou, Y., Chen, Y., and Gu, J. (2018). fastp: an ultra-fast all-in-one FASTQ preprocessor. *Bioinformatics*. **34**: i884-i890.
36. Kim, D., Langmead, B., and Salzberg, S. L. (2015). HISAT: a fast spliced aligner with low memory requirements. *Nat Methods*. **12**: 357-360.
37. Pertea, M., Pertea, G. M., Antonescu, C. M., Chang, T. C., Mendell, J. T., and Salzberg, S. L. (2015). StringTie enables improved reconstruction of a transcriptome from RNA-seq reads. *Nat Biotechnol*. **33**: 290-295.
38. Li, B., and Dewey, C. N. (2011). RSEM: accurate transcript quantification from RNA-Seq data with or without a reference genome. *BMC Bioinformatics*. **12**: 323.
39. Robinson, M. D., McCarthy, D. J., and Smyth, G. K. (2010). edgeR: a Bioconductor package for differential expression analysis of digital gene expression data. *Bioinformatics*.

26: 139-140.

40. Rupp, R. A., Snider, L., and Weintraub, H. (1994). *Xenopus* embryos regulate the nuclear localization of XMyoD. *Genes Dev*. **8**: 1311-1323.
41. Wang, W., Hu, B., Yuan, D., Liu, Y., Che, R., Hu, Y., Ou, S., Liu, Y., Zhang, Z., Wang, H., et al. (2018). Expression of the nitrate transporter gene *OsNRT1.1A*/*OsNPF6.3* confers high yield and early maturation in rice. *Plant Cell*. 3**0**: 638-651.
42. Ma, L., Qin, DB., Sun, L., Zhang, K., Yu, X., Dang, AK., Hou, S., Zhao, X., Yang, Y., Wang, Y., et al. (2025). SALT OVERLY SENSITIVE2 and AMMONIUM TRANSPORTER1;1 contribute to plant salt tolerance by maintaining ammonium uptake. *Plant Cell*. **37**: koaf034.
43. Jefferson, R. A., Kavanagh, T. A., and Bevan, M. W. (1987). GUS fusions: beta-glucuronidase as a sensitive and versatile gene fusion marker in higher plants. *Embo j*. **6**: 3901-3907.
44. Liu, Y, Q., Hu, B., and Chu, C, J. (2016). ^{15}N-nitrate uptake activity and root-to-shoot transport assay in rice. *Bio Protocol*. **6**: 1897.
45. Gupta, S. K., Joshi, F. M., Limbachiya, D., and Gupta, M. K. (2014). 3DNA: A Tool for DNA Sculpting. *ArXiv*. abs/1405.4118.
46. Zhang, C., Fang, H., Wang, J., Tao, H., Wang, D., Qin, M., He, F., Wang, R., Wang, GL., Ning, Y. (2024). The rice E3 ubiquitin ligase-transcription factor module targets two trypsin inhibitors to enhance broad-spectrum disease resistance. *Dev Cell*. **59**: 2017-2033.e5.

Acknowledgements

We thank Professor Lanqin Xia (Institute of Crop Sciences, Chinese Academy of Agricultural Sciences) for assistance with wheat transformation, Professor Yiping Tong (Institute of Genetics and Developmental Biology, China) for providing NILs materials, Professor Yuanming Zhang and PhD student Ying Chen (Huazhong Agricultural University) for helping with candidate-gene and genome-wide association studies, Professor Yun Zhou and PhD Shenglong Bai (Henan University) for helping map the *TaNPF7.6-A1* alleles geographical

distribution. We are also grateful to Professor Yiping Tong, and Yuanming Zhang for their helpfully critical reading and valuable suggestions for the manuscript. This work was financially supported by the National Key Research and Development Program of China (2022YFD1200204), the Key Scientific and Technological Project of Henan Province (262102111135), the Science and Technology R&D Program Joint Fund of Henan Province (Grant No. 222301420025), the 'First-class Project' of Shennong Laboratory (SN01-2022-01), the earmarked fund for China Agriculture Research System (CARS-03).

Author contributions

W.G.X. coordinated the project, conceived and designed the experiments; D.J. and C.J.P. performed the experiments and analyzed the data. D.J. wrote the original draft. Y.L., C.G., Y.H.F., X.Y.Z., Z.Y.W., X.N.W., and L.H. assisted with the experimental operations and contributed valuable discussions; X.L.Q reviewed and revised this paper; All authors have read the article and approved the submitted version.

Competing interests

The authors declare no competing interests.

Additional information

Supplementary information: Figures S1-S15 and Datas S1-S13.

Correspondence and requests for materials should be addressed to Weigang X

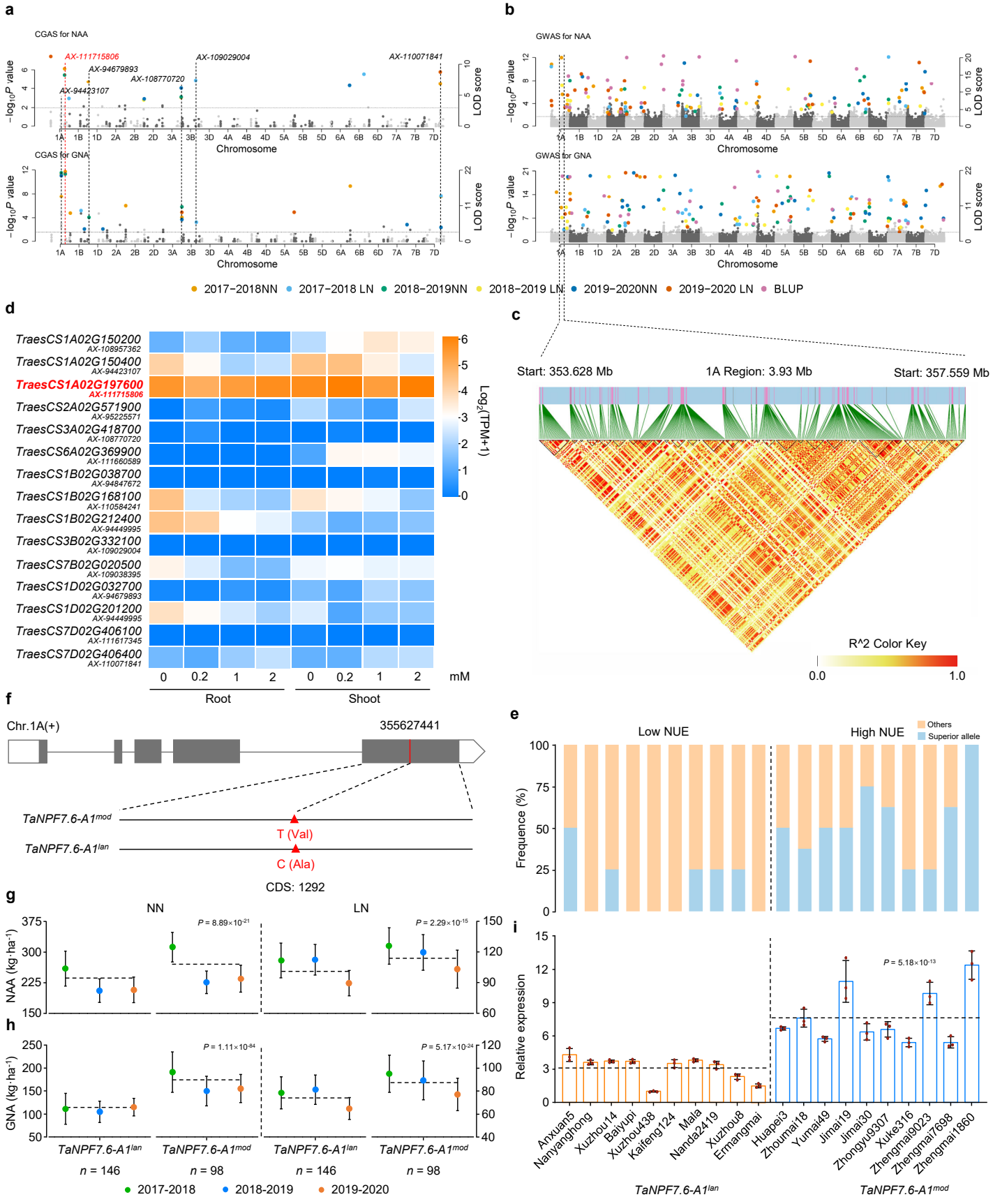

a
CGAS for NAA
AX-111715806
AX-94679893
AX-94423107
AX-108770720
AX-109029004
AX-110071841
−log10P value
LOD score
Chromosome
CGAS for GNA
b
GWAS for NAA
GWAS for GNA
2017−2018NN
2017−2018 LN
2018−2019NN
2018−2019 LN
2019−2020NN
2019−2020 LN
BLUP
d
TraesCS1A02G150200
AX-108957362
TraesCS1A02G150400
AX-94423107
TraesCS1A02G197600
AX-111715806
TraesCS2A02G571900
AX-95225571
TraesCS3A02G418700
AX-108770720
TraesCS6A02G369900
AX-111660589
TraesCS1B02G038700
AX-94847672
TraesCS1B02G168100
AX-110584241
TraesCS1B02G212400
AX-94449995
TraesCS3B02G332100
AX-109029004
TraesCS7B02G020500
AX-109038395
TraesCS1D02G032700
AX-94679893
TraesCS1D02G201200
AX-94449995
TraesCS7D02G406100
AX-111617345
TraesCS7D02G406400
AX-110071841
Log2(TPM+1)
0 0.2 1 2 0 0.2 1 2 mM
Root
Shoot
c
Start: 353.628 Mb
1A Region: 3.93 Mb
Start: 357.559 Mb
R^2 Color Key
0.0
1.0
f
Chr.1A(+)
355627441
TaNPF7.6-A1mod
T (Val)
TaNPF7.6-A1lan
C (Ala)
CDS: 1292
e
Low NUE
High NUE
Others
Superior allele
Frequence (%)
g
NN
LN
NAA (kg·ha−1)
P = 8.89×10−21
P = 2.29×10−15
h
GNA (kg·ha−1)
P = 1.11×10−84
P = 5.17×10−24
TaNPF7.6-A1lan
TaNPF7.6-A1mod
n = 146
n = 98
n = 146
n = 98
2017-2018
2018-2019
2019-2020
i
Relative expression
P = 5.18×10−13
Anxuan5
Nanyanghong
Xuzhou14
Baiyupi
Xuzhou438
Kaifeng124
Mala
Nanda2419
Xuzhou8
Ermangmai
Huapei3
Zhoumai18
Yumai49
Jimai19
Jimai30
Zhongyu9307
Xuke316
Zhengmai9023
Zhengmai7698
Zhengmai1860
TaNPF7.6-A1lan
TaNPF7.6-A1mod

Fig 1. *TaNPF7.6-A1* alleles are associated with nitrogen use efficiency in wheat. a CGAS scan for NAA and GNA. The dashed lines indicate that 6 loci were stably identified across multiple environments and traits, the red dashed line represents *AX-111715806* on chromosome 1A with the largest r^2. **b** GWAS results for NAA and GNA. Colored dots indicate the genome-wide significance loci. The black dashed lines indicate the candidate region (353.628-357.559 Mb) for significant marker-trait associations on chromosome 1A. **c** LD heatmap surrounding the 353.628-357.559 Mb candidate region. **d** Heatmap of the relative expression of the fifteen candidate genes under four nitrogen supply conditions (0, 0.2, 1, and 2 mM NO_3^-) based on RNA sequencing of wheat seedlings root and shoot. The color key (blue to orange) represents fold changes of gene expression. The first candidate gene functionally analyzed in this study is highlighted in red. **e** Distribution of superior and inferior *NPF* alleles in twenty different NUE wheat varieties. Orange boxes represent the inferior alleles, blue boxes represent the superior alleles. **f** Gene structure and natural allelic variation at the coding sequence region of *TaNPF7.6-A1*, red indicates alleles that cause one amino acid substitution, gray bars: the coding region, white bars: the UTRs. **g-h** Comparison of the NAA(**g**), GNA(**h**) between *TaNPF7.6-A1* two alleles under NN and LN fields in 2017-2018 (green, left), 2018-2019 (blue, middle), and 2019-2020 (orange, right). *TaNPF7.6-A1*^{lan} with 146 varieties carrying the corresponding allele, while *TaNPF7.6-A1*^{mod} has 98 varieties. The data used for calculation were derived from experiments shown in Fig 1**a**-**b**. **i** The relative expression of *TaNPF7.6-A1* in twenty wheat varieties with different NUE. Values represent mean ± SD derived from three individual plants. In **g**-**i**, the dotted lines represent the average values of all varieties with the same allele, respectively, *P* values were calculated with two-tailed Student's *t* test. Source data are provided as a Source Data file.

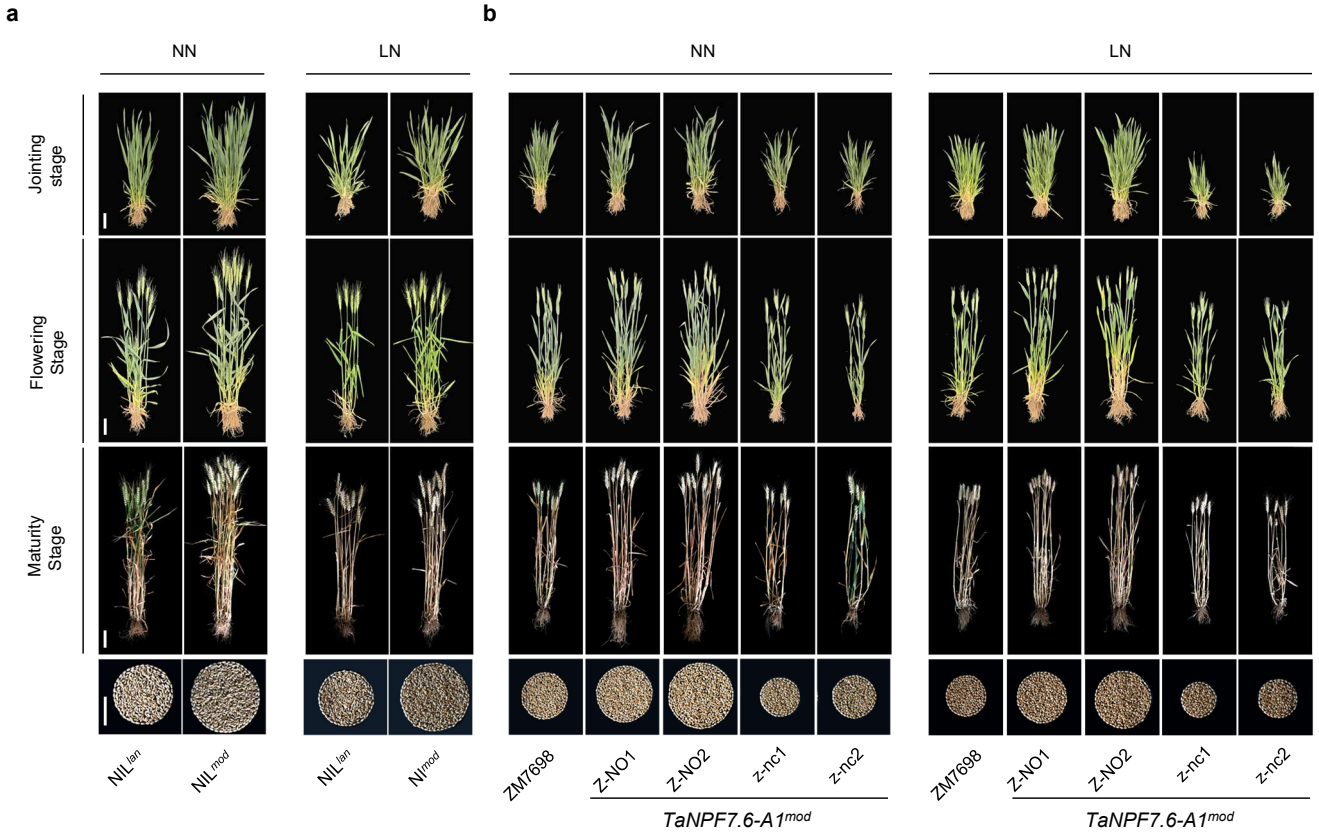


Table1. Aboveground dry weight and N accumulation of the NILs, wiid type (ZM7698), Z-NO lines and z-nc lines

Line	Jointing stage				Flowering Stage				Maturity Stage			
	Aboveground dry weight g/plant		Total N g/plant		Straw N g/plant		Spik N g/plant		Straw N g/plant		Grain N g/plant	
	NN	LN	NN	LN	NN	LN	NN	LN	NN	LN	NN	LN
NIL^{lan}	6.38	4.46	0.116	0.041	0.313	0.085	0.054	0.034	0.103	0.066	0.392	0.221
NIL^{mod}	7.43**	5.48**	0.163**	0.063**	0.400**	0.130**	0.077**	0.046**	0.100	0.063	0.490**	0.273**
WT	5.18^{c}	4.63^{c}	0.109^{c}	0.047^{c}	0.227^{b}	0.068^{b}	0.040^{b}	0.020^{b}	0.099^{a}	0.058^{a}	0.430^{b}	0.243^{b}
Z-NO1	6.57^{b}	5.41^{b}	0.144^{b}	0.062^{b}	0.303^{a}	0.082^{a}	0.057^{a}	0.027^{a}	0.092^{ab}	0.055^{ab}	0.541^{a}	0.291^{a}
Z-NO2	7.30^{a}	5.85^{a}	0.165^{a}	0.074^{a}	0.313^{a}	0.085^{a}	0.060^{a}	0.027^{a}	0.086^{b}	0.053^{ab}	0.539^{a}	0.305^{a}
z-nc1	4.47^{d}	3.56^{d}	0.088^{d}	0.032^{d}	0.142^{c}	0.045^{c}	0.028^{c}	0.013^{c}	0.102^{a}	0.050^{b}	0.319^{c}	0.136^{c}
z-nc2	4.19^{e}	3.26^{e}	0.077^{e}	0.030^{e}	0.147^{c}	0.046^{c}	0.030^{c}	0.013^{c}	0.099^{a}	0.054^{ab}	0.314^{c}	0.171^{c}

Values are presented as means ± SDs. (n = 20 plants, *P < 0.05, **P < 0.01, Student's t-test. Different letters indicate significant differences (P < 0.05, one-way ANOVA, Duncan's new multiple range test).

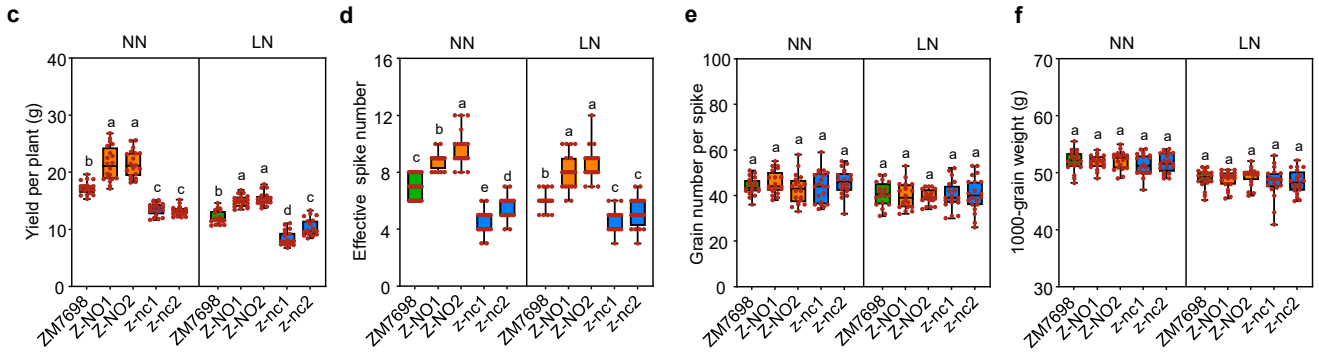


Fig 2. High *TaNPF7.6-A1^{mod}* levels confer advantage in NUE and wheat grain yield. **a-b** The phenotypes of NILs(**a**), ZM7698, the *TaNPF7.6-A1^{mod}* overexpression (Z-NO) lines, the *TaNPF7.6-A1^{mod}* knockout (z-nc) lines(**b**) under the jointing stage, the flowering stage and the maturity stage, and yield per plant at the maturity stage under LN and NN fields (2023-2024). Scale bars, 10 cm. NN, Normal nitrogen treatment; LN, Low nitrogen treatment. **c-f** Yield per plant(**c**), effective spike number(**d**), grain number per spike(**e**) and 1000-grain weight(**f**) in ZM7698, Z-NO and z-nc lines under low-density conditions. (n = 20 plants). In **c-f**, different letters indicate significant differences ($P < 0.05$, one-way ANOVA, Duncan's new multiple range test). Source data are provided as a Source Data file.

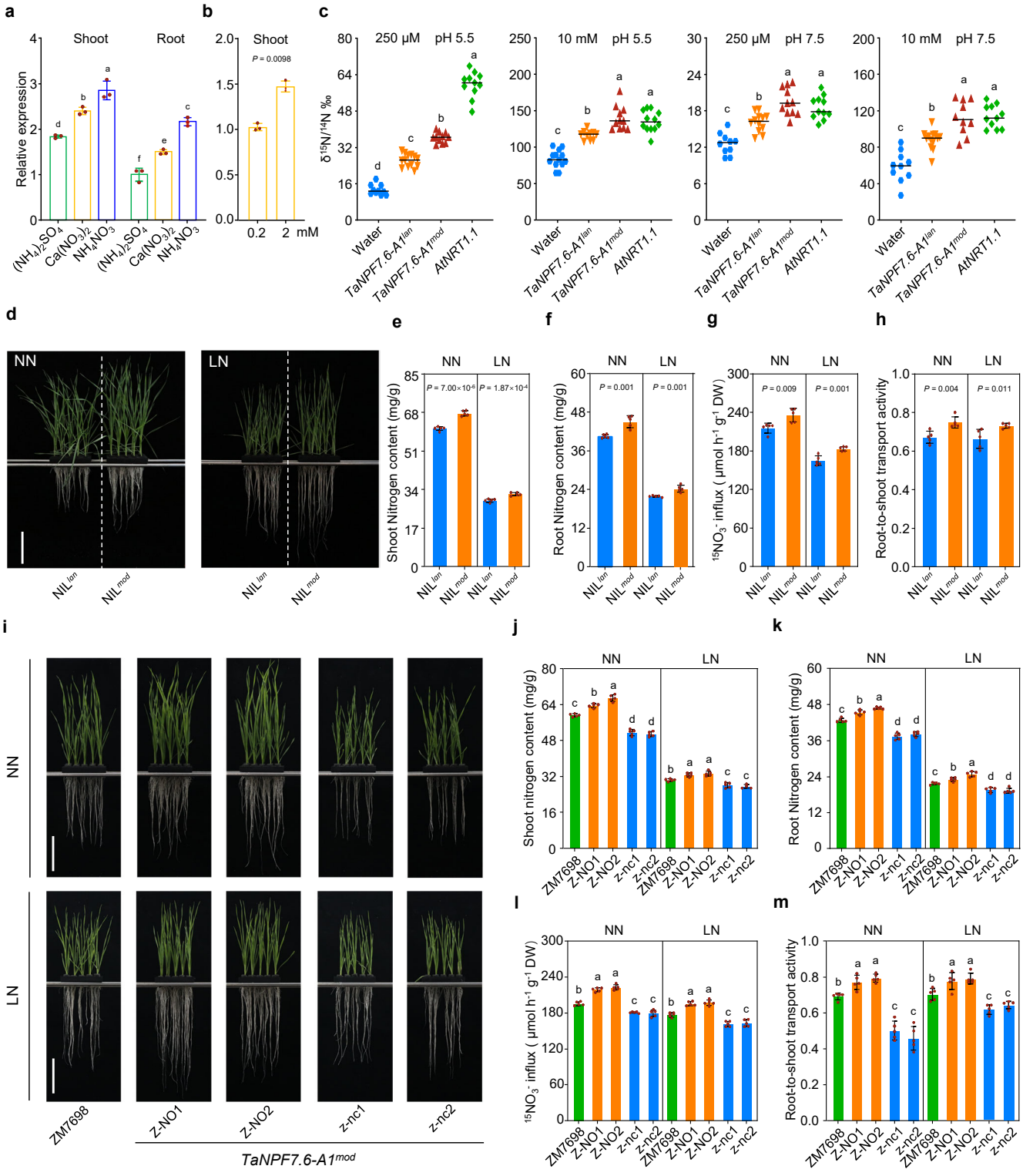

a
b
c
Shoot
Root
Relative expression
(NH4)2SO4
Ca(NO3)2
NH4NO3
P = 0.0098
0.2
2 mM
250 μM pH 5.5
10 mM pH 5.5
250 μM pH 7.5
10 mM pH 7.5
δ15N/14N ‰
Water
TaNPF7.6-A1lan
TaNPF7.6-A1mod
AtNRT1.1
d
e
f
g
h
NN
LN
NILlan
NILmod
Shoot Nitrogen content (mg/g)
Root Nitrogen content (mg/g)
15NO3- influx (μmol h-1 g-1 DW)
Root-to-shoot transport activity
P = 7.00×10-6
P = 1.87×10-4
P = 0.001
P = 0.009
P = 0.004
P = 0.011
i
j
k
l
m
ZM7698
Z-NO1
Z-NO2
z-nc1
z-nc2
TaNPF7.6-A1mod
Shoot nitrogen content (mg/g)

Fig 3. *TaNPF7.6-A1^{mod}* positively regulates wheat nitrate uptake and translocation capacity. a-b Expression patterns of *TaNPF7.6-A1^{mod}* in 2-week-old wheat seedlings, shoots and roots under three N source (2 mM) hydroponic cultivation conditions(**a**), and shoots under two $Ca(NO_3)_2$ supply (0.1 and 1 mM) conditions(**b**). *n* = three individual wheat seedlings of shoot and root tissues. **c** Two *TaNPF7.6-A1* alleles show nitrate transport activity in vitro. Nitrate uptake assay in *Xenopus laevis* oocytes injected with water, *TaNPF7.6-A1^{lan}*, *TaNPF7.6-A1^{mod}* and *AtNRT1.1* using ^{15}N-nitrate. *AtNRT1.1* was used as the positive control, water was used as the negative control, at least ten replicates were performed for each sample. **d** Growth of NILs in 2-week hydroponic culture under NN (2 mM nitrate) and LN (0.2 mM nitrate) conditions, scale bar = 10 cm. **e-f** Total nitrogen content of NILs shoots(**e**), and roots(**f**) in 2-week hydroponic culture under NN (2 mM nitrate) or LN (0.2 mM nitrate) conditions. *n* = 5 biological replicates for each line. **g-h** $^{15}N–NO_3^-$ uptake(**g**), and root-to-shoot transport activities(**h**) of NILs when exposed to either NN (2 mM nitrate) or LN (0.2 mM nitrate) ^{15}N-labeled KNO_3 for 3 h. *n* = 5. **i** Growth of ZM7698, Z-NO lines and z-nc lines in 2-week hydroponic culture under NN or LN conditions, scale bar = 10 cm. **j-k** Total nitrogen content of ZM7698, Z-NO lines and z-nc lines shoots (**j**), roots (**k**) in 2-week hydroponic culture under NN or LN conditions. *n* = 5 biological replicates for each line. **l-m** $^{15}N–NO_3^-$ uptake (**l**) and root-to-shoot transport activities (**m**) of ZM7698, Z-NO lines, z-nc lines when exposed to either NN or LN ^{15}N-labeled KNO_3 for 3 h. *n* = 5. In **a**-**c**, **e**-**h**, and **j**-**m**, data are mean ± SD. **b**, **e**-**h** Student's *t*-test. **a**, **c**, **j**-**m** Different letters indicate significant differences ($P < 0.05$, one-way ANOVA, Duncan's new multiple range test). Source data are provided as a Source Data file.

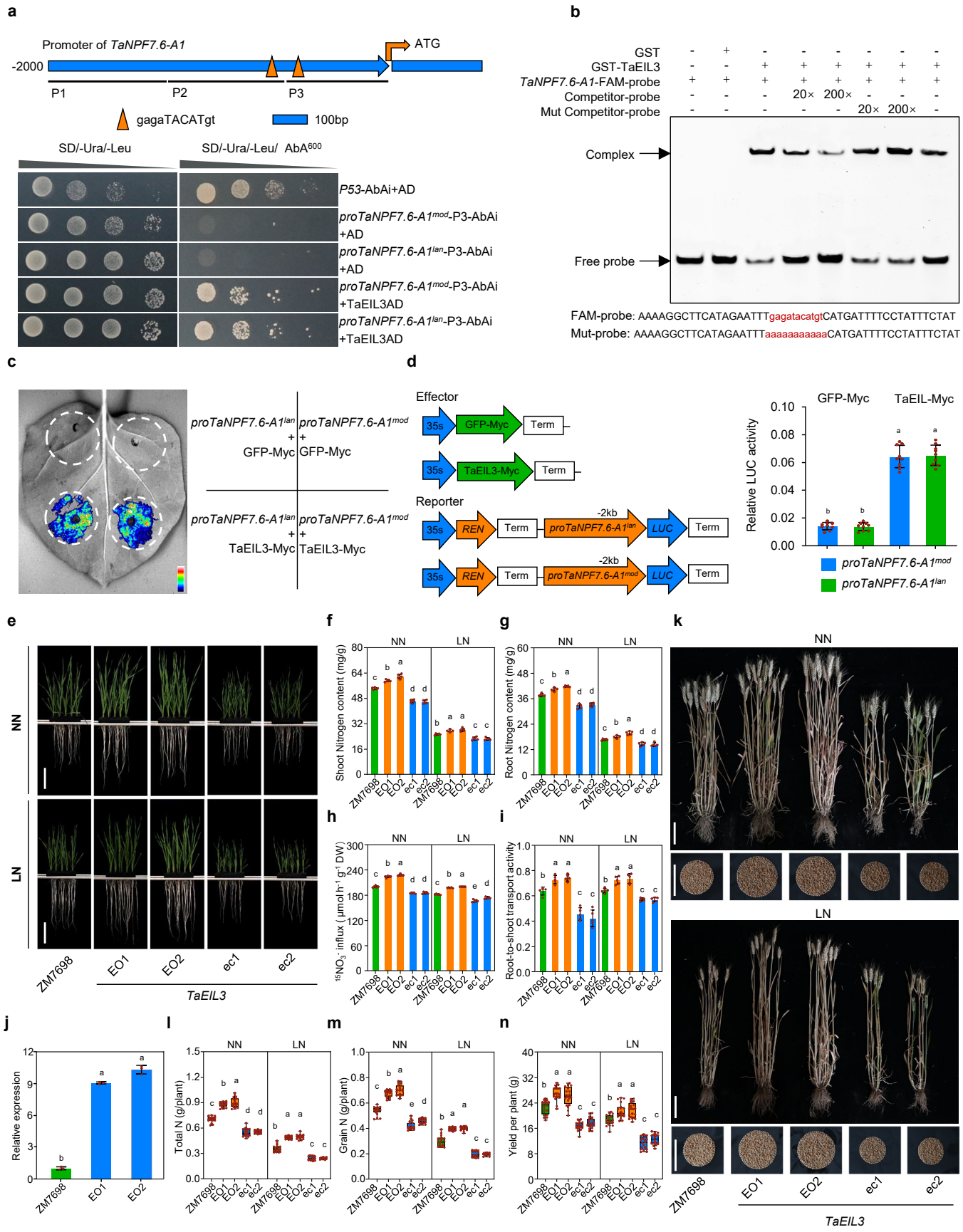

a
Promoter of TaNPF7.6-A1
-2000
ATG
P1
P2
P3
gagaTACATgt
100bp
SD/-Ura/-Leu
SD/-Ura/-Leu/ AbA600
P53-AbAi+AD
proTaNPF7.6-A1mod-P3-AbAi +AD
proTaNPF7.6-A1lan-P3-AbAi +AD
proTaNPF7.6-A1mod-P3-AbAi +TaEIL3AD
proTaNPF7.6-A1lan-P3-AbAi +TaEIL3AD
b
GST
GST-TaEIL3
TaNPF7.6-A1-FAM-probe
Competitor-probe
Mut Competitor-probe
Complex
Free probe
FAM-probe: AAAAGGCTTCATAGAATTTgagatacatgtCATGATTTTCCTATTTCTAT
Mut-probe: AAAAGGCTTCATAGAATTTaaaaaaaaaaaCATGATTTTCCTATTTCTAT
c
proTaNPF7.6-A1lan + GFP-Myc
proTaNPF7.6-A1mod + GFP-Myc
proTaNPF7.6-A1lan + TaEIL3-Myc
proTaNPF7.6-A1mod + TaEIL3-Myc
d
Effector
35s
GFP-Myc
Term
TaEIL3-Myc
Reporter
REN
-2kb
proTaNPF7.6-A1lan
proTaNPF7.6-A1mod
LUC
Relative LUC activity
e
NN
LN
ZM7698
EO1
EO2
ec1
ec2
TaEIL3
f
Shoot Nitrogen content (mg/g)
g
Root Nitrogen content (mg/g)
h
15NO3- influx (μmol h-1 g-1 DW)
i
Root-to-shoot transport activity
j
Relative expression
l
Total N (g/plant)
m
Grain N (g/plant)
n
Yield per plant (g)
k

Fig 4. TaEIL3 regulates NUE by directly promoting the expression of *TaNPF7.6-A1*. **a** TaEIL3 could bind to the P3 of *TaNPF7.6-A1*^{mod} and *TaNPF7.6-A1*^{lan} promoter via Y1H assay. **b** EMSA analysis of TaEIL3 binding to *TaNPF7.6-A1* promoter. The unlabeled probe containing wide type or mutated motif from P3 fragment was used as competitor. "+" and "−" indicate the presence and absence, respectively, of the corresponding probes and proteins. **c** Dual luciferase reporter assays showing transcriptional regulation of TaEIL3 on *TaNPF7.6-A1*^{mod} and *TaNPF7.6-A1*^{lan}. **d** Schematic diagrams of the reporters and effectors used in the transient transactivation assays and transient dual-luciferase reporter assays demonstrated that TaEIL3 activates the expression of *TaNPF7.6-A1*^{mod} and *TaNPF7.6-A1*^{lan}. The relative luciferase activities were calculated by normalizing the luciferase (LUC) values against renilla luciferase (REN). $n = 9$. **e** Growth of ZM7698, *TaEIL3* overexpression (EO) lines and *TaEIL3* knockout (ec) lines in 2-week hydroponic culture under NN (2 mM nitrate) or LN (0.2 mM nitrate) conditions, scale bar = 10 cm. **f-g** Total nitrogen content in shoots (**f**) and roots (**g**) of ZM7698, *TaEIL3* overexpression (EO) lines and *TaEIL3* knockout (ec) lines in 2-week hydroponic culture under NN (2 mM nitrate) or LN (0.2 mM nitrate) conditions. $n = 5$. **h-i** $^{15}N–NO_3^-$ uptake(**h**) and root-to-shoot transport activities (**i**) of ZM7698, EO lines and ec lines when exposed to either NN (2 mM nitrate) or LN (0.2 mM nitrate) ^{15}N-labeled KNO_3 for 3 h. $n = 5$. **j** Relative expression of *TaNPF7.6-A1* in ZM7698 and *TaEIL3* overexpression lines. Values represent mean ± SD derived from shoot tissues from three individual wheat seedlings. **k** The phenotypes of ZM7698, EO lines and ec lines at the maturity stage under LN and NN fields (2024-2025). Scale bar = 10 cm. **l-n** Aboveground total N accumulation (**l**), grain N accumulation (**m**), yield per plant (**n**) in ZM7698, EO lines and ec lines ($n = 20$). In **d**, **f-j**, and **l-n**, different letters indicate significant differences ($P < 0.05$, one-way ANOVA, Duncan's new multiple range test). Source data are provided as a Source Data file.

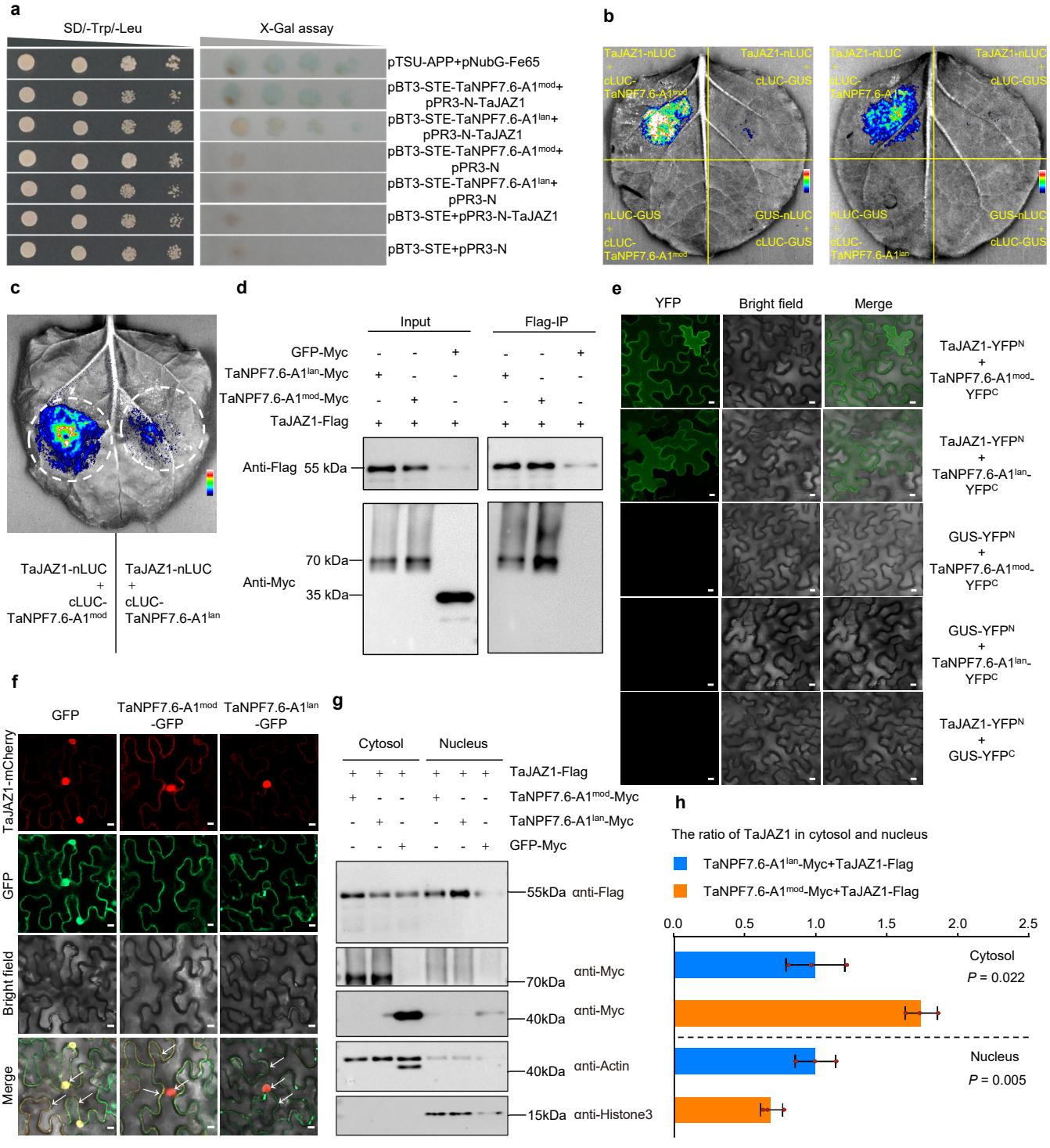

a
SD/-Trp/-Leu
X-Gal assay
pTSU-APP+pNubG-Fe65
pBT3-STE-TaNPF7.6-A1mod+ pPR3-N-TaJAZ1
pBT3-STE-TaNPF7.6-A1lan+ pPR3-N-TaJAZ1
pBT3-STE-TaNPF7.6-A1mod+ pPR3-N
pBT3-STE-TaNPF7.6-A1lan+ pPR3-N
pBT3-STE+pPR3-N-TaJAZ1
pBT3-STE+pPR3-N
b
TaJAZ1-nLUC + cLUC-TaNPF7.6-A1mod
TaJAZ1-nLUC + cLUC-GUS
nLUC-GUS + cLUC-TaNPF7.6-A1mod
GUS-nLUC + cLUC-GUS
TaJAZ1-nLUC + cLUC-TaNPF7.6-A1lan
nLUC-GUS + cLUC-TaNPF7.6-A1lan
c
TaJAZ1-nLUC + cLUC-TaNPF7.6-A1mod
TaJAZ1-nLUC + cLUC-TaNPF7.6-A1lan
d
Input
Flag-IP
GFP-Myc
TaNPF7.6-A1lan-Myc
TaNPF7.6-A1mod-Myc
TaJAZ1-Flag
Anti-Flag 55 kDa
70 kDa
35 kDa
Anti-Myc
e
YFP
Bright field
Merge
TaJAZ1-YFPN + TaNPF7.6-A1mod-YFPC
TaJAZ1-YFPN + TaNPF7.6-A1lan-YFPC
GUS-YFPN + TaNPF7.6-A1mod-YFPC
GUS-YFPN + TaNPF7.6-A1lan-YFPC
TaJAZ1-YFPN + GUS-YFPC
f
GFP
TaNPF7.6-A1mod -GFP
TaNPF7.6-A1lan -GFP
TaJAZ1-mCherry
GFP
Bright field
Merge
g
Cytosol
Nucleus
TaJAZ1-Flag
TaNPF7.6-A1mod-Myc
TaNPF7.6-A1lan-Myc
GFP-Myc
55kDa anti-Flag
70kDa anti-Myc
40kDa anti-Myc
40kDa anti-Actin
15kDa anti-Histone3
h
The ratio of TaJAZ1 in cytosol and nucleus
TaNPF7.6-A1lan-Myc+TaJAZ1-Flag
TaNPF7.6-A1mod-Myc+TaJAZ1-Flag
0.0
0.5
1.0
1.5
2.0
2.5
Cytosol
P = 0.022
Nucleus
P = 0.005

Fig 5. Natural variants in TaNPF7.6-A1 influence interaction strength with TaJAZ1 and alter TaJAZ1 nuclear-cytoplasmic distribution. a Verification of protein interaction by split-ubiquitin yeast system. All the transformation colonies were grown on the SD/-trp/-Leu and SD/-Leu/-trp/-his/-Ade plates, followed by the examination of LacZ reporter gene with X-Gal as a substrate, the combination of pTSU-APP and pNubG-Fe65 was used as the positive control. **b-c** Luciferase complementation imaging (LCI) assay shows that TaJAZ1 interacts with TaNPF7.6-A1^{mod} and TaNPF7.6-A1^{lan}, and indicates that TaJAZ1 interacts more strongly with TaNPF7.6-A1^{mod}. **d** Co-immunoprecipitation (Co-IP) assay showing the physical interactions of TaJAZ1 with TaNPF7.6-A1^{mod} or TaNPF7.6-A1^{lan}. *N. benthamiana* leaves were transformed by injection of the *Agrobacterium* Gv3101 cells containing TaNPF7.6-A1^{mod}-Myc and TaJAZ1-Flag, TaNPF7.6-A1^{lan}-Myc and TaJAZ1-Flag plasmids. Total proteins were immunoprecipitated with Flag, and the immunoblots were probed with the anti-Flag and anti-Myc antibodies, respectively. **e** Bimolecular fluorescence complementation (BiFC) assay revealing the interaction of TaJAZ1 with TaNPF7.6-A1^{mod} or TaNPF7.6-A1^{lan} in tobacco leaves. Scale bar, 10 μm. **f** TaNPF7.6-A1^{mod} or TaNPF7.6-A1^{lan} co-localized with TaJAZ1 in *N. benthamiana* leaves. Scale bar, 10 μm. **g** TaNPF7.6-A1 and TaJAZ1 extracted from the cytosol and nucleus components of *N. benthamiana* leaf tissues were detected by western blotting with anti-Flag or anti-Myc antibodies. Cytosol-localized protein Actin and nucleus-localized protein Histone 3 were detected using their monoclonal antibodies and served as positive controls of cytosol and nucleus components, respectively. The experiment was repeated three times independently with similar results. **h** Ratio of TaJAZ1 in cytosol and nucleus in **g**. Error bars represent the mean ± SD (n = 3). P values were calculated with two-tailed Student's t test. Source data are provided as a Source Data file.

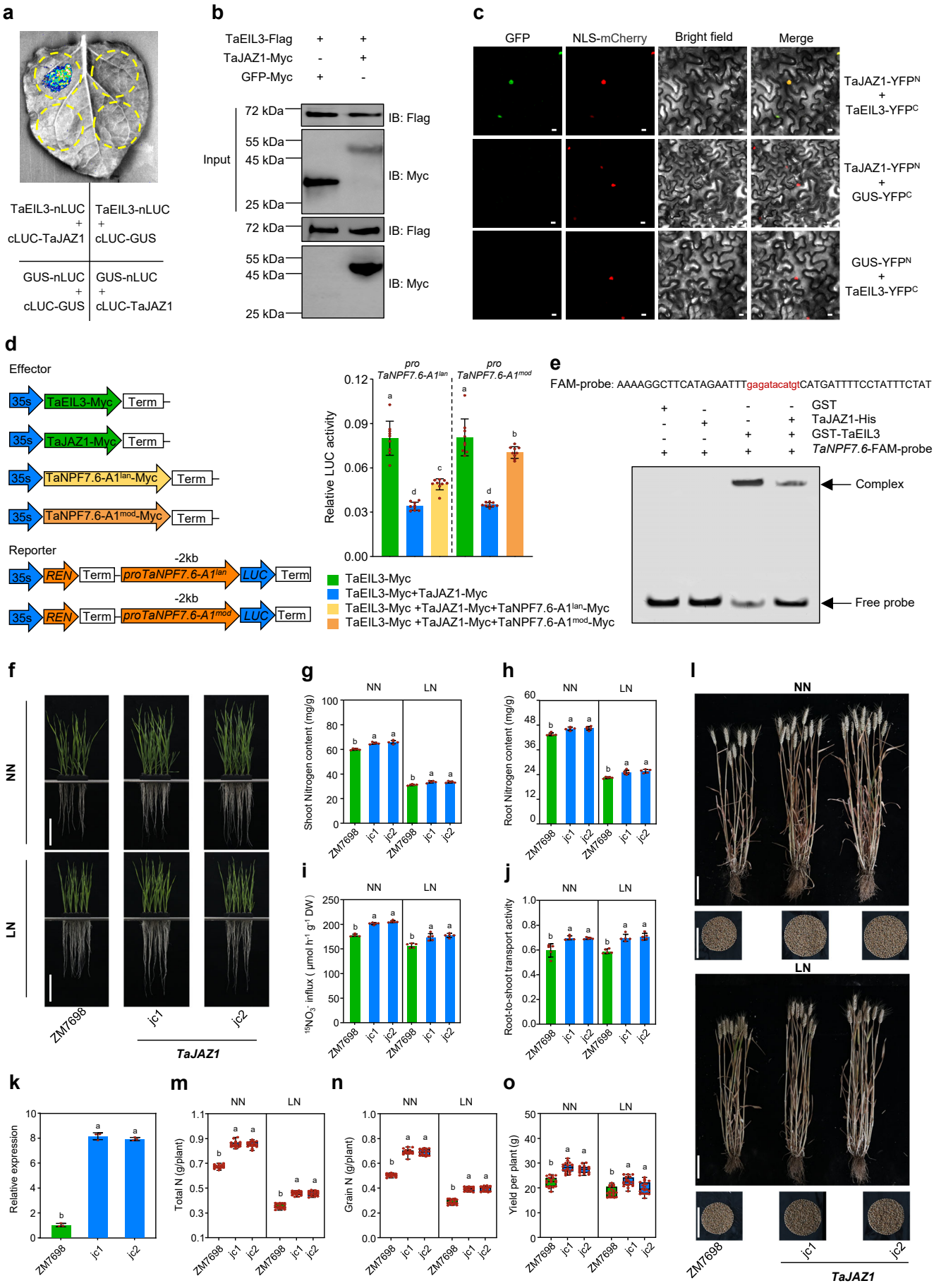

a
TaEIL3-nLUC + cLUC-TaJAZ1
TaEIL3-nLUC + cLUC-GUS
GUS-nLUC + cLUC-GUS
GUS-nLUC + cLUC-TaJAZ1
b
TaEIL3-Flag + +
TaJAZ1-Myc - +
GFP-Myc + -
Input
72 kDa
55 kDa
45 kDa
25 kDa
IB: Flag
IB: Myc
c
GFP
NLS-mCherry
Bright field
Merge
TaJAZ1-YFPN + TaEIL3-YFPC
TaJAZ1-YFPN + GUS-YFPC
GUS-YFPN + TaEIL3-YFPC
d
Effector
35s
TaEIL3-Myc
TaJAZ1-Myc
TaNPF7.6-A1lan-Myc
TaNPF7.6-A1mod-Myc
Term
Reporter
-2kb
REN
LUC
proTaNPF7.6-A1lan
proTaNPF7.6-A1mod
Relative LUC activity
TaEIL3-Myc
TaEIL3-Myc+TaJAZ1-Myc
TaEIL3-Myc +TaJAZ1-Myc+TaNPF7.6-A1lan-Myc
TaEIL3-Myc +TaJAZ1-Myc+TaNPF7.6-A1mod-Myc
e
FAM-probe: AAAAGGCTTCATAGAATTTgagatacatgtCATGATTTTCCTATTTCTAT
GST
TaJAZ1-His
GST-TaEIL3
TaNPF7.6-FAM-probe
Complex
Free probe
f
NN
LN
ZM7698
jc1
jc2
TaJAZ1
g
Shoot Nitrogen content (mg/g)
h
Root Nitrogen content (mg/g)
i
15NO3- influx (μmol h-1 g-1 DW)
j
Root-to-shoot transport activity
k
Relative expression
l
m
Total N (g/plant)
n
Grain N (g/plant)
o
Yield per plant (g)

Fig6. TaJAZ1 physically interacts with TaEIL3 and interferes with the regulation of *TaNPF7.6-A1* two alleles by TaEIL3, which compromises wheat NUE. a LCI validating the interaction between TaJAZ1 and TaEIL3. **b** Co-IP assay showing the interaction between TaJAZ1 and TaEIL3 in *N. benthamiana* leaves co-infiltrated with the constructs TaEIL3-Flag and TaJAZ1-Myc. **c** BiFC assay revealing the interaction of TaJAZ1 with TaEIL3 in the nucleus. Scale bar, 10 μm. **d** Dual-LUC detection of the effect of TaJAZ1 on the transcriptional activation of *TaNPF7.6-A1*^{mod} and *TaNPF7.6-A1*^{lan} by TaEIL3, with or without TaNPF7.6-A1^{mod} and TaNPF7.6-A1^{lan}. The relative luciferase activities were calculated by normalizing the LUC values against REN. $n = 9$. **e** EMSA analysis of TaEIL3 and TaJAZ1 binding to *TaNPF7.6-A1* promoter. "+" and "−" indicate the presence or absence of the corresponding probes and proteins, respectively. **f** Growth of ZM7698 and *TaJAZ1* knockout (jc) lines in 2-week hydroponic culture under NN (2 mM nitrate) or LN (0.2 mM nitrate) conditions, scale bar = 10 cm. **g-h** Total nitrogen content in shoots (**g**), roots (**h**) of ZM7698 and jc lines in 2-week hydroponic culture under NN (2 mM nitrate) or LN (0.2 mM nitrate) conditions. $n = 5$ biological replicates for each line. **i-j** $^{15}N–NO_3^-$ uptake(**i**), root-to-shoot transport activities (**j**) of ZM7698 and jc lines when exposed to either NN (2 mM nitrate) or LN (0.2 mM nitrate) ^{15}N-labeled KNO_3 for 3 h. $n = 5$ biological replicates for each line). **k** Relative expression of *TaNPF7.6-A1* in ZM7698 and *TaJAZ1* knockout lines. Values represent mean ± SD derived from shoot tissues from three individual wheat seedlings. **l** The phenotypes of ZM7698 and jc lines at the maturity stage under LN and NN fields (2024-2025). Scale bar = 10 cm. **m-o** Aboveground total N accumulation (**m**), grain N accumulation (**n**), yield per plant (**o**) in ZM7698 and jc lines ($n = 20$) In **d**, **g**-**k**, and **m**-**o**, data are mean ± SD, different letters indicate significant differences ($P < 0.05$, one-way ANOVA, Duncan's new multiple range test). Source data are provided as a Source Data file.

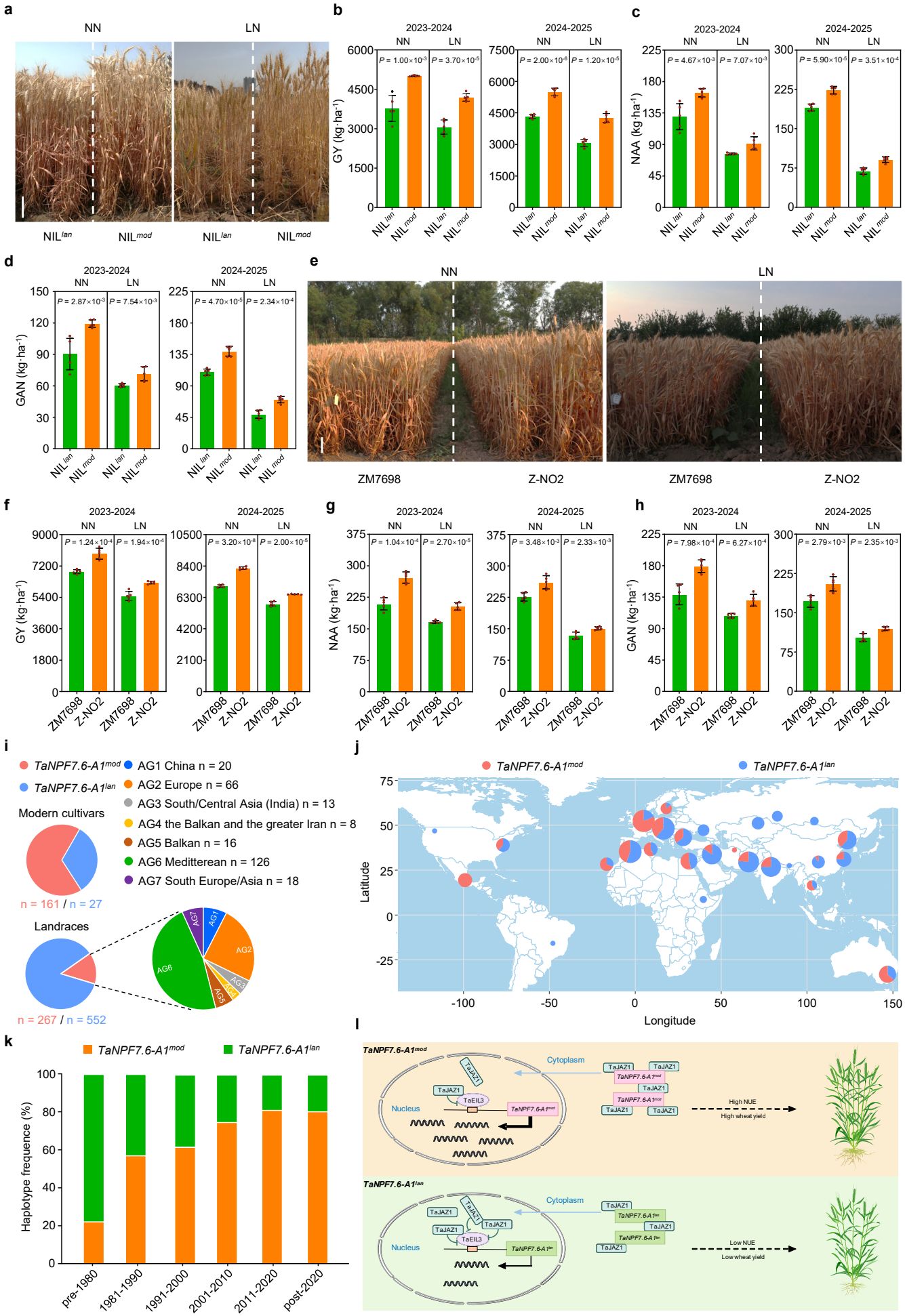

a
NN
LN
NIL^lan
NIL^mod
b
2023-2024
2024-2025
GY (kg·ha⁻¹)
c
NAA (kg·ha⁻¹)
d
GAN (kg·ha⁻¹)
e
ZM7698
Z-NO2
f
g
h
i
TaNPF7.6-A1^mod
TaNPF7.6-A1^lan
Modern cultivars
n = 161 / n = 27
Landraces
n = 267 / n = 552
AG1 China n = 20
AG2 Europe n = 66
AG3 South/Central Asia (India) n = 13
AG4 the Balkan and the greater Iran n = 8
AG5 Balkan n = 16
AG6 Mediterean n = 126
AG7 South Europe/Asia n = 18
j
Latitude
Longitude
k
Haplotype frequence (%)
pre-1980
1981-1990
1991-2000
2001-2010
2011-2020
post-2020
l
Cytoplasm
Nucleus
TaJAZ1
TaEIL3
High NUE
High wheat yield
Low NUE
Low wheat yield

Fig7. Breeding potential and geographical distribution of *TaNPF7.6-A1^{mod}*. a Field trials of NIL^{mod} and NIL^{lan} plants in NN and LN fields under high-density conditions. Scale bar, 10 cm. **b-d** GY(**b**), NAA(**c**), GAN(**d**) of NIL^{mod} and NIL^{lan} for two consecutive years (2023-2025). *P* values were calculated with two-tailed Student's *t* test. **e** The images represent ZM7698 and Z-NO2 plants in NN and LN fields under high-density conditions. Scale bar, 10 cm. **f-h** GY(**f**), NAA(**g**), GAN(**h**) of ZM7698 and Z-NO2 plants for two consecutive years (2023-2025). *P* values were calculated with two-tailed Student's *t* test. Source data are provided as a Source Data file. **i** Frequency distribution analysis of *TaNPF7.6-A1* alleles in 819 Watkins landraces and 188 modern cultivars. **j** Geographical distribution of 1007 wheat varieties based on longitude and latitude, the data also used in Fig 7I. **k** Changes in the frequency of *TaNPF7.6-A1* alleles in Chinese modern cultivars during different Chinese wheat breeding periods (pre-1980 to post-2020). **g** A proposed working model for *TaEIL3-TaJAZ1-TaNPF7.6-A1* regulating wheat NUE and grain yield. Differences in the expression of *TaNPF7.6-A1* alleles do not stem from transcriptional regulation but from variations in protein interaction strength. *TaNPF7.6-A1^{mod}* displays elevated transcription levels, positively influenced by TaEIL3, and inhibited by TaJAZ1 interact with TaEIL3 in the nucleus. TaJAZ1 exhibits a stronger affinity for TaNPF7.6-A1^{mod} compared to TaNPF7.6-A1^{lan}, resulting in enhanced translocation of TaJAZ1 from the nucleus to the cytoplasm in TaNPF7.6-A1^{mod}. Within the nucleus, TaJAZ1 interacts with TaEIL3, thereby repressing the transcriptional activity of *TaNPF7.6-A1*. This unique interaction mechanism serves as the primary determinant of the differential gene expression observed between the two alleles, ultimately resulting in variations in NUE in wheat.

Supplementary Files

This is a list of supplementary files associated with this preprint. Click to download.

- SupplementalData5.xlsx
- DescriptionofAdditionalSupplementaryData.pdf
- SupplementalData3.xlsx
- SupplementalData1.xlsx
- SupplementalData10.xlsx
- SupplementalData11.xlsx
- SupplementalData9.xlsx
- SupplementalFigures.pdf
- SupplementalData6.xlsx
- SupplementalData2.xlsx
- SupplementalData8.xlsx
- SupplementalData12.xlsx
- SupplementalData13.xlsx
- SupplementalData7.xlsx
- SupplementalData4.xlsx
- reportingsummary.pdf